Article

Cell Reports

# Single-Cell Deconvolution of Fibroblast Heterogeneity in Mouse Pulmonary Fibrosis

## Graphical Abstract

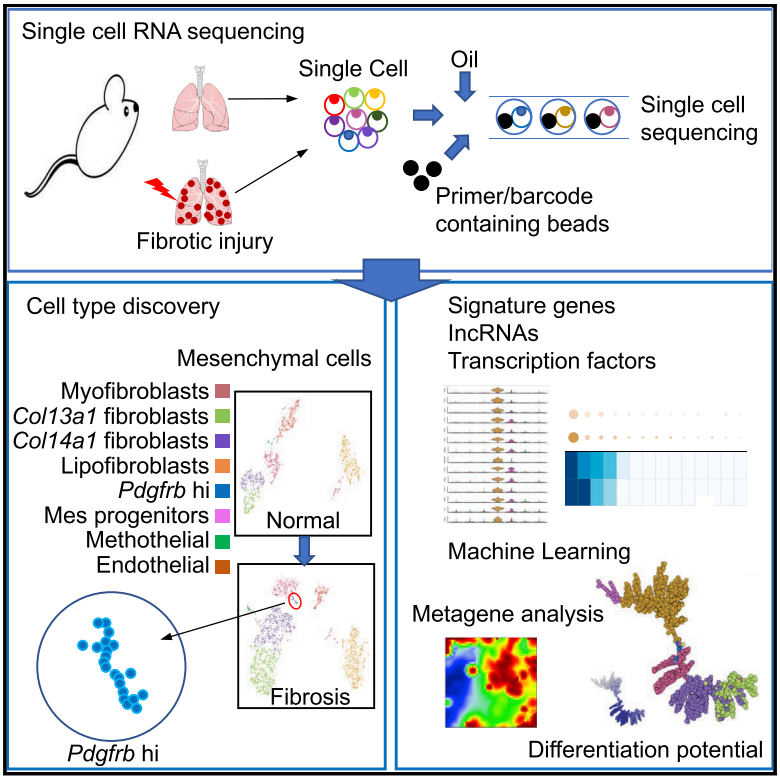


## Authors

Ting Xie, Yizhou Wang, Nan Deng, ..., Jiurong Liang, Paul W. Noble, Dianhua Jiang

## Correspondence

ting.xie@cshs.org (T.X.), paul.noble@cshs.org (P.W.N.), dianhua.jiang@cshs.org (D.J.)

## In Brief

Xie et al. have analyzed mesenchymal cell subpopulations at single-cell resolution and have demonstrated known subtypes and a newly emerging subtype during pulmonary fibrosis in mouse lung.

## Highlights

- Distinct MC subtypes were defined by single-cell transcriptome analysis
- Lipofibroblasts were identified
- Fibrotic *Pdgfrb* high MC subtype emerges post-injury
- Integrative analysis of MC trajectories was constructed by machine learning

## Data and Software Availability

GSE104154

Xie et al., 2018, Cell Reports *22*, 3625–3640
March 27, 2018 
https://doi.org/10.1016/j.celrep.2018.03.010

CellPress

Cell Reports
Article



# Single-Cell Deconvolution of Fibroblast Heterogeneity in Mouse Pulmonary Fibrosis

Ting Xie,[1,*] Yizhou Wang,[2] Nan Deng,[3] Guanling Huang,[1] Forough Taghavifar,[1] Yan Geng,[1] Ningshan Liu,[1] Vrishika Kulur,[1] Changfu Yao,[1] Peter Chen,[1] Zhengqiu Liu,[3] Barry Stripp,[1] Jie Tang,[2] Jiurong Liang,[1] Paul W. Noble,[1,*] and Dianhua Jiang[1,4,*]

[1]Department of Medicine, Division of Pulmonary and Critical Care Medicine, Women's Guild Lung Institute, Cedars-Sinai Medical Center, Los Angeles, CA 90048, USA
[2]Genomics Core, Department of Biomedical Sciences, Cedars-Sinai Medical Center, Los Angeles, CA 90048, USA
[3]Samuel Oschin Comprehensive Cancer Institute, Cedars-Sinai Medical Center, Los Angeles, CA 90048, USA
[4]Lead Contact
*Correspondence: ting.xie@cshs.org (T.X.), paul.noble@cshs.org (P.W.N.), dianhua.jiang@cshs.org (D.J.)
https://doi.org/10.1016/j.celrep.2018.03.010

## SUMMARY

**Fibroblast heterogeneity has long been recognized in mouse and human lungs, homeostasis, and disease states. However, there is no common consensus on fibroblast subtypes, lineages, biological properties, signaling, and plasticity, which severely hampers our understanding of the mechanisms of fibrosis. To comprehensively classify fibroblast populations in the lung using an unbiased approach, single-cell RNA sequencing was performed with mesenchymal preparations from either uninjured or bleomycin-treated mouse lungs. Single-cell transcriptome analyses classified and defined six mesenchymal cell types in normal lung and seven in fibrotic lung. Furthermore, delineation of their differentiation trajectory was achieved by a machine learning method. This collection of single-cell transcriptomes and the distinct classification of fibroblast subsets provide a new resource for understanding the fibroblast landscape and the roles of fibroblasts in fibrotic diseases.**

## INTRODUCTION

Fibrosis is an evolutionary body strategy to rapidly close and repair wounds (Bochaton-Piallat et al., 2016; Gurtner et al., 2008). In the lung, fibrosis occurs when there is an ongoing epithelial injury (Liang et al., 2016; Thomas et al., 2002). Fibrosis in patients with idiopathic pulmonary fibrosis (IPF) results in persistent and relentlessly progressive lung scarring (Thannickal et al., 2014; Thum, 2014; Tzouvelekis and Kaminski, 2015), which leads to ~40,000 deaths every year in the US. The major effector cells in this process are the mesenchymal cells (MCs) (Li et al., 2011). MCs are believed to consist of multiple subtypes that are being intensively investigated (Kumar et al., 2014; Lee et al., 2017; Xie et al., 2016; Zepp et al., 2017), but it is unclear how many mesenchymal subtypes exist and how they differ from or are related to one another, and their cellular biology is poorly defined. Thus, these limitations hinder severely our ability to understand the cellular events and the molecular signaling pathways in the distinct subsets of fibroblasts in fibrogenesis, and to develop precise cellular models and animal models of lung fibrosis.

Pulmonary MCs are suggested to be extremely heterogeneous in IPF (Jordana et al., 1988) and in mouse models (Rock et al., 2011), suggesting that they could be derived from different cell types, represent different stages of activation, or may be influenced by the surrounding milieu. MC clones separated by Thy1 seem to have different morphology, growth characteristics, display of antigens, and collagen and fibronectin production (Derdak et al., 1992). Subsets of MCs distinguished by Pdgfrα expression were reported to express different levels of α-smooth muscle actin (αSMA) (Kimani et al., 2009). The regional airway MCs were suspected to be distinct from the distal lung MCs in terms of morphology, collagen and αSMA expression, and proliferation (Kotaru et al., 2006). Using genetic lineage tools to characterize lung MCs has provided some insights into subtypes. *Fgf10* lineage MCs (El Agha et al., 2012); pericytes trace labeled with *NG2*, *FoxJ1*, or *Foxd1* (Hung et al., 2013; Rock et al., 2011); or *Plin2*-traced lipofibroblasts (El Agha et al., 2017) were suggested to contribute to αSMA-expressing myofibroblasts and various MC subsets. We recently reported that *Tbx4*-lineage cells compose a large fibroblast population within the lung, including αSMA$^+$, Col1α1$^+$, NG2$^+$, vimentin$^+$, desmin$^+$, Pdgfrα$^+$, and Pdgfrβ$^+$ fibroblasts (Xie et al., 2016). These data suggest the existence of cellular subpopulations of fibroblasts, which vary with anatomical locations, gene expression, and cell surface markers. However, the enumeration of cell types and their definition can be controversial based on restricted markers available to identify, isolate, and manipulate. Biased morphology, physical properties, localization, molecular markers, functions, and developmental origins would alter the assignment of diversification and cellular differentiation for mesenchymal subtypes. Therefore, a systematic map of evolutionary pulmonary mesenchymal heterogeneity in both steady-state and pathological conditions remains unexposed.

To overcome these challenges, efforts have been made to systematically classify lung MCs. The Lung Gene Expression in Single-Cell (LungGENS) program separated MCs into proliferative mesenchymal progenitor, myofibroblast/smooth

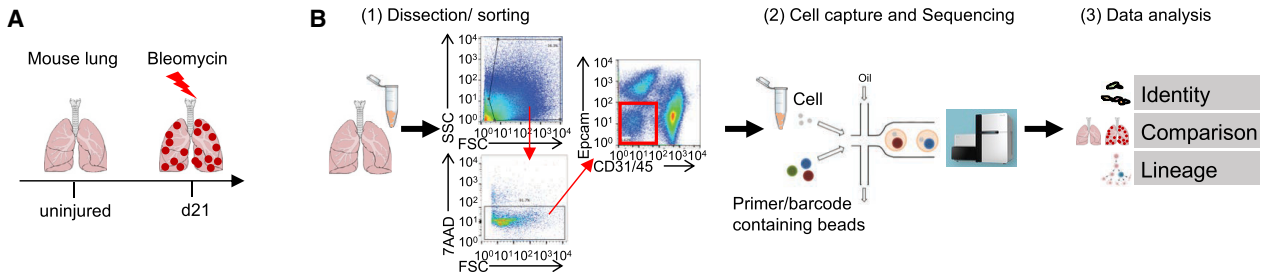


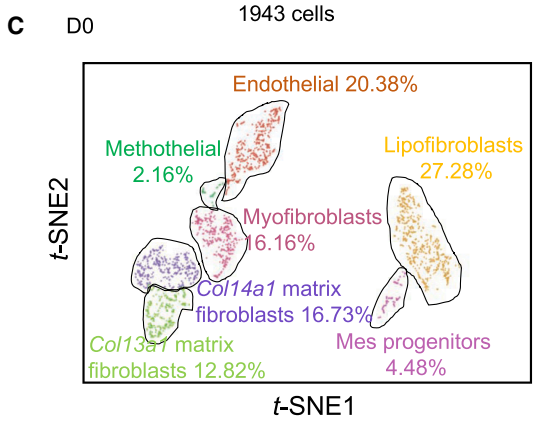


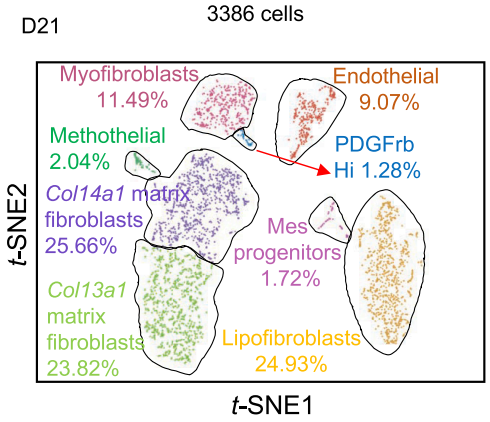


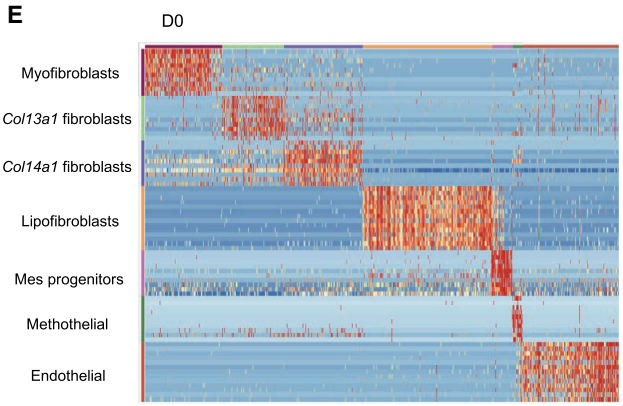


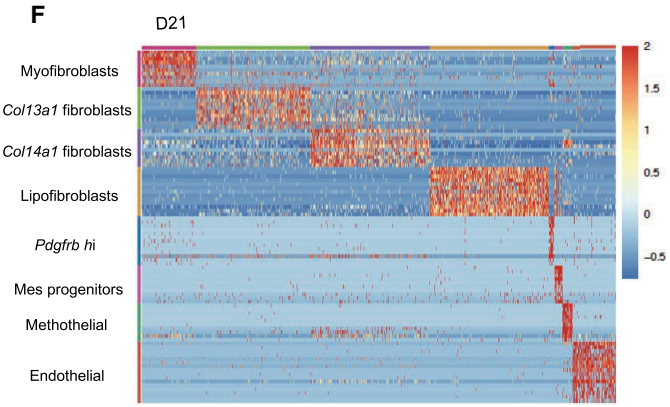


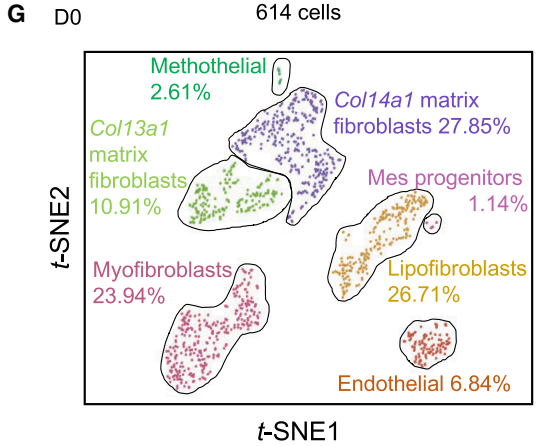


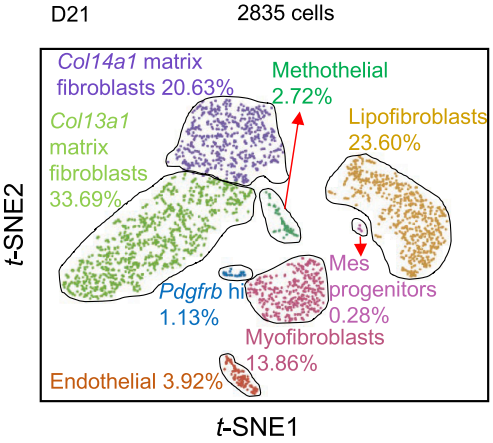


(legend on next page)

muscle, pericyte, intermediate fibroblast 1 and 2 and matrix fibroblast on embryonic (E) 16.5, and FB (LipoFibroblast/Matrix Fibroblast) and myofibroblast/smooth muscle on E18.5 and postnatal mouse lungs by single-cell RNA sequencing (scRNA-seq) analysis using the Fluidigm C1 platform (Du et al., 2015). However, the numbers of fibroblasts included in the studies were small because of the limitation of the C1 platform. To conquer some of these obstacles, we used an unbiased approach: Drop-Seq single-cell RNA-seq (scRNA-seq; 10x Genomics) with much larger numbers of MCs to better assess the diversity of pulmonary MCs, leading to the identification of new subtypes of fibroblasts, and refine their existing classifications. We further assessed the signature genes, enriched extracellular and soluble protein coded genes, key transcription factors, and, notably, expressed long non-coding RNAs (lncRNAs) for each subtype. In addition, pseudo-time analysis was used to delineate the mesenchymal cellular paths of differentiation. Overall, our analysis provides a comprehensive map of the subtypes of the stromal taxonomy in steady-state in adult mice and fibrotic lung.

## RESULTS

### Classification of Mesenchymal Heterogeneity by scRNA-Seq in Normal and Fibrotic Mouse Lung Tissues

We set out to comprehensively identify and define subpopulations of the MCs between normal and fibrotic lung tissues. We treated *αSMA-GFP;Tbx4-Cre;Rosa26-tdTomato* mice with bleomycin and harvested the lungs after injury (Figure 1A). We obtained enriched MCs by fluorescence-activated cell sorting (FACS) Epcam$^{-}$CD31$^{-}$45$^{-}$ cells from single lung homogenates and performed scRNA-seq using the 10x Genomics Chromium platform (Figure 1B). We profiled 1,943 cells from normal mouse lung and 3,386 cells from fibrotic *αSMA-GFP;Tbx4-Cre;Rosa26-tdTomato* mouse lung. We visualized the cells in two dimensions according to their expression profiles by t-distributed stochastic neighborhood embedding (t-SNE) projections. Six subtypes as MCs in normal lung and seven subtypes in fibrotic lung were well segregated (Figures 1C and 1D). Endothelial cells also were included in the analysis. The other cell types such as epithelial cells contaminated during flow sorting were minimal and easily identifiable, and were eliminated from further analysis. We tentatively classified mesenchymal populations based on their preferential or distinctive marker expression and relations to known cell types. The compositions of these clusters were myofibroblasts, 16% in normal and 11% in fibrotic lung; *Col13a1* matrix fibroblasts, 13% in normal and 24% in fibrotic lung; *Col14a1* matrix fibroblasts, 17% in normal and 26% in fibrotic lung; lipofibroblasts, 27% in normal and 25% in fibrotic lung; mesenchymal progenitors, 5% in normal and 2% in fibrotic lung; mesothelial cells, 2% in normal and 2% in fibrotic lung; and endothelial cells, 20% in normal and 9% in fibrotic lung. A new *Pdgfrb* high (hi) subpopulation appeared only in the fibrotic lung, which comprised ~1% of all MCs (Figures 1C and 1D). Heatmaps of normalized MC profiles revealed normalized expression of the top variable genes in each MC subtype (Figures 1E and 1F). We further analyzed tdTomato (tdT)$^{+}$GFP$^{+}$ cells from *αSMA-GFP;Tbx4-Cre;Rosa26-tdTomato* mice to confirm the MC subtypes (Figures 1G and 1H). As expected, these subtypes and the patterns of composition were consistently reproduced in the analyses of 614 MCs in normal and 2,835 MCs in fibrotic tdT$^{+}$GFP$^{+}$ cells. Together, these unbiased analyses delineated the fibroblast heterogeneity in the adult mouse lungs and further identified mesenchymal subpopulation changes during lung fibrogenesis.

### Single-Cell Profiling of Myofibroblasts

Using known marker genes for myofibroblasts, including *Acta2* (Hinz et al., 2007), *Myh11* (Hsia et al., 2016), and *Tagln* (Du et al., 2015; Robin et al., 2013) (Figures 2A–2C), a myofibroblast cluster was readily identified. Top 10 genes were highly and specifically expressed in myofibroblasts and absent or much less expressed in other MC subtypes, providing a series of novel markers that can distinguish myofibroblasts from other fibroblasts under both normal and fibrotic conditions (Figures 2D and 2E). The expression levels of the top highly expressed lncRNAs in myofibroblasts; the top 36 most abundant expressed genes, including extracellular and plasma membrane coding genes; and the most abundant transcription factors were analyzed and compared between normal and fibrotic myofibroblast subtypes (Figures 2F–2I). Among the newly identified putative myofibroblast markers, several are of particular interest. *Hhip*, which has been reported to be involved in maintaining normal lung function and alveolar structures (Lao et al., 2016), is the highest specifically expressing gene in the myofibroblast subtype. *Aspn* has been reported to be significantly expressed in IPF lung samples (Leng et al., 2013). *Mustn1*, which has been reported to be expressed in skeletal muscle, is believed to be an essential regulator of myogenic differentiation and myofusion (Liu et al., 2010). All three of these were better markers of myofibroblasts than was *Acta2*, which is consistent with the results of a recent report (Sun et al., 2016). Junb is a component of transcription complex AP1 (Andreucci et al., 2002). AP1, which has been shown to play a key

**Figure 1. Clustering of Mesenchymal Cells by Single-Cell RNA Sequencing**

(A) Sketch of bleomycin-induced pulmonary fibrosis mouse model.

(B) Workflow depicts rapid dissociation and sorting of MCs from lung tissue for generating scRNA transcriptome profiles.

(C and D) 2D visualization of single-cell clustering of MC profiles inferred from RNA-seq data for all MCs in normal (C) and fibrotic (D) *αSMA-GFP;Tbx4-Cre;Rosa26-tdTomato* lung samples. Six major classes of MCs in normal lung and seven major classes of MCs in fibrotic lung were detected. Endothelial cells also were included in the analysis. The percentage of each cell population was indicated. Colored bar coded as indicated.

(E and F) Heat maps of MC normalized signal show MC subtypes changes by top genes (columns) for individual MC subtype cells (rows) in normal (E) and fibrotic (F) *αSMA-GFP;Tbx4-Cre;Rosa26-tdTomato* lung samples.

(G and H) Clustering plots depicting single-cell RNA-seq datasets for normal (G) and fibrotic (H) Tbx4-lineage$^{+}$αSMA$^{+}$ MCs acquired from marker-based fluorescence-activated cell sorting (FACS).

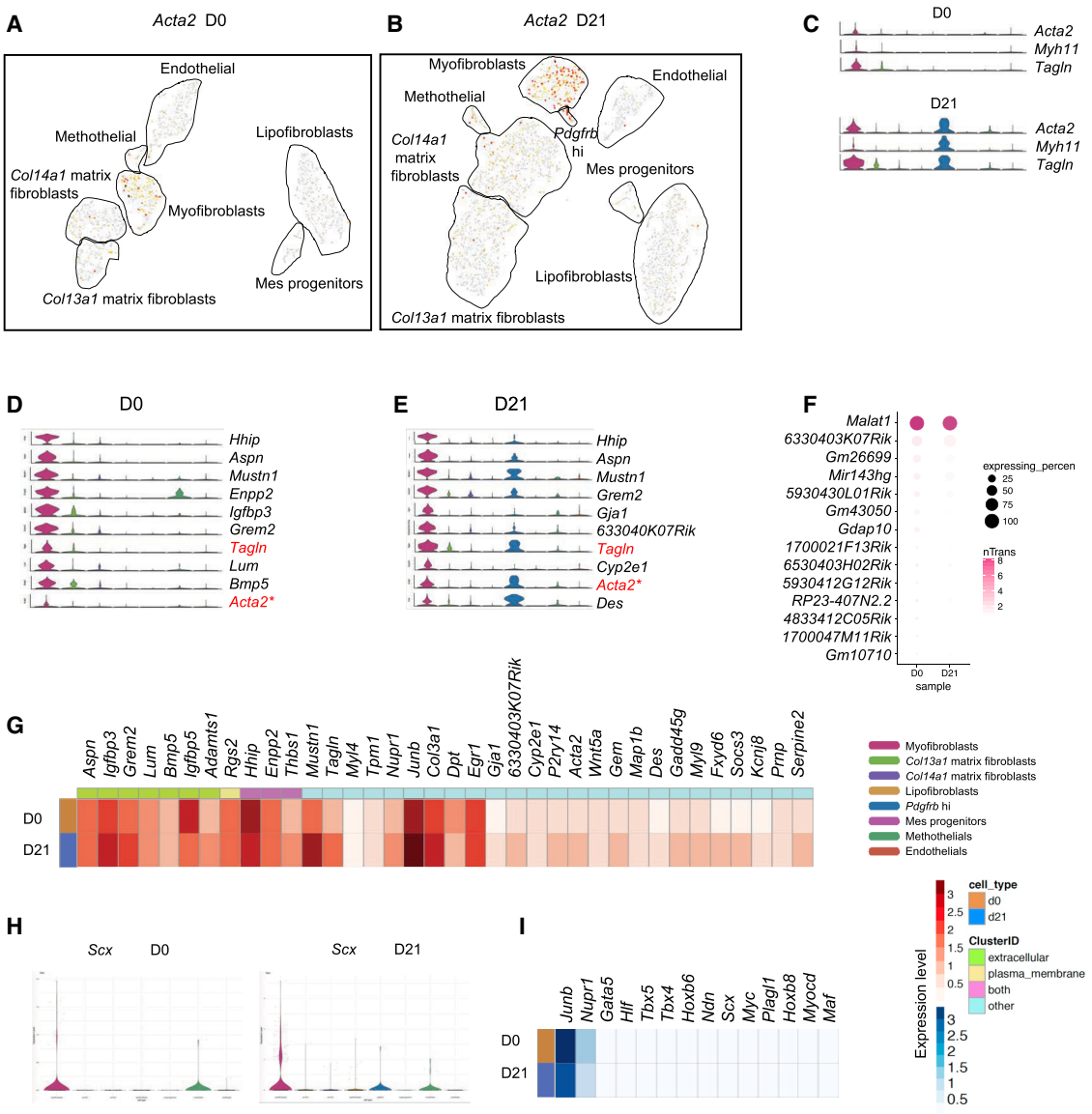


**Figure 2. Transcriptional Profile of Myofibroblasts**

(A and B) Expression patterns of *Acta2* (D0, A; D21, B) in representation as in Figures 1C and 1D.

(C) Violin plots showing known myofibroblast markers *Acta2*, *Myh11*, and *Tagln* gene expression across all MC clusters.

(D and E) Representative markers were distinct in normal (D) and fibrotic (E) myofibroblast clusters predicted in the scRNA-seq data.

(F) Top lncRNAs enriched in myofibroblasts. The size of each circle depicts the percentage of cells in the subtype in which the marker was detected, and its color depicts the average transcript count in expressing cells (nTrans).

(G) Heatmap of top significant genes, including extracellular and plasma membrane genes in this subtype. Rows correspond to normal (D0) and fibrotic (D21) myofibroblast subtypes, and columns correspond to the mean of the single-cell gene expression signature arranged by expression locations.

(H) Signature transcription factor *Scx* expression across all MC subtypes.

(I) Enrichment patterns of transcription factors in the myofibroblast subtype.

role in fibrotic diseases, and *Scx*, a transcription factor reported to be a critical regulator of the cardiac fibroblast/myofibroblast phenotype (Bagchi et al., 2016), are showing up as the most distinctive transcription factors of myofibroblast subtypes in both normal and fibrotic conditions. These analyses identified novel markers and transcription networks in the myofibroblast subtype.

## Transcriptional Signature Associated With *Col13a1* Matrix Fibroblasts

Matrix fibroblasts express signature genes associated with extracellular matrix and cell adhesion. We found that these *Col1a1* highly expressing matrix fibroblasts clustered together (Figures S1A and S1B). *Col13a1* and *Col14a1* are highly discriminative markers within the matrix fibroblast clusters, segregating

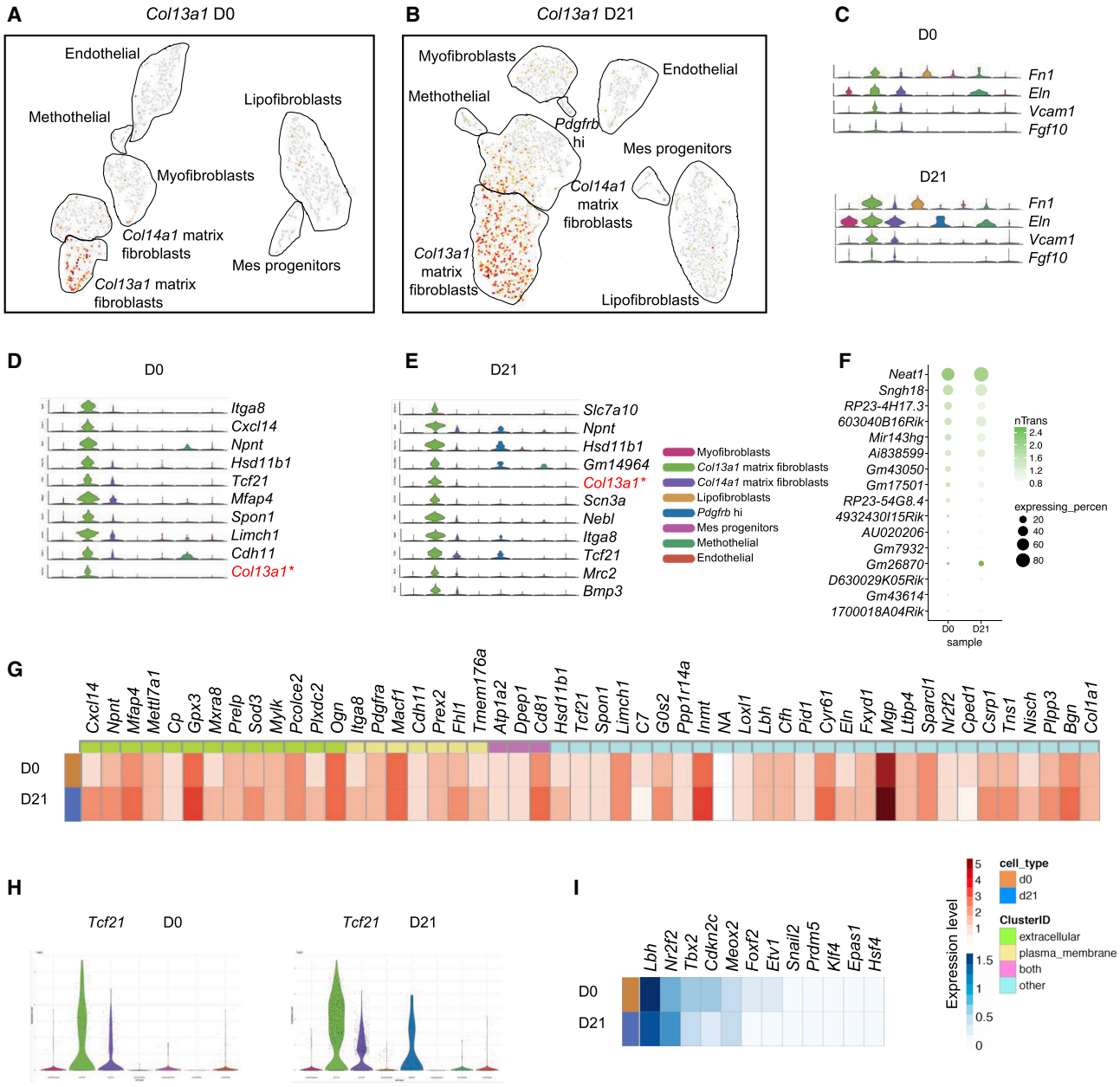


**Figure 3. Matrix Fibroblast Subtype Enriched in *Col13a1***

(A and B) Visualization of normal (A) and fibrotic (B) *Col13a1* gene expression using a t-SNE plot.

(C) Expression patterns of known matrix fibroblast marker genes across MC subtypes.

(D and E) Core distinct expressed genes in *Col13a1* subtype from both normal (D) and fibrotic (E) lungs were indicated by violin plots.

(F) lncRNAs identified in the *Col13a1* subtype.

(G) Heatmap of significantly expressed genes with the indication of their cellular locations was compared between normal and fibrotic *Col13a1* subtypes.

(H) Violin plot of *Tcf21* gene expression, which is highlighted in the *Col13a1* subtype.

(I) Heatmap showing changes in top transcription factors between normal and fibrotic *Col13a1* subtypes.

them into two distinct subtypes. We refer to these subsets henceforth as *Col13a1* and *Col14a1* matrix fibroblasts (Figures 3A and 3B). Previously reported matrix fibroblast markers are dominantly expressed in both *Col13a1* and *Col14a1* matrix fibroblasts (Figure 3C). *Col13a1* matrix fibroblasts were accurately delineated by *Itga8*, *Cxcl14*, *Npnt*, and other top signature genes in both normal and fibrotic lung (Figures 3D and 3E). Most of the highly expressed lncRNAs were analyzed and ordered by the range of their expression (Figure 3F), with *Neat1* being the most abundantly expressed lncRNA. The top 50 significantly expressed genes were listed with discrimination of the extracellular and plasma membrane expressing genes, and their expression

levels were depicted as heatmaps (Figure 3G). Chemokine *Cxcl14* is the most distinct extracellular expressed gene in *Col13a1* matrix fibroblasts. Plasma membrane associated gene *Itga8* can uniquely delineate *Col13a1* matrix fibroblasts. Both *Cxcl14* and *Igta8* are increased in fibrotic *Col13a1* matrix fibroblasts. Transcription factor *Tcf21* strongly marked the *Col13a1* matrix fibroblasts, with more abundant expression at the fibrotic phase (Figure 3H). Tcf21 has been used to lineage trace resident cardiac fibroblasts during pathologic remodeling (Xiang et al., 2017). Other top transcription factors include *Lbh*, *Nr2f2*, *Tbx2*, and *Meox2* (Figure 3I).

### Delineation of *Col14a1* Matrix Fibroblasts

Unlike *Col13a1* matrix fibroblasts, *Col14a1* matrix fibroblasts distinguish themselves by harboring a unique set of significant genes, including *Pi16*, *Mmp3*, *Cygb*, and *Rtp4* (Figures 4A–4D). *Meg3* and *Snhg18* are the most abundant lncRNAs expressed in the *Col14a1* matrix fibroblasts. The percentage of the cells expressing *Meg3* in *Col14a1* matrix fibroblasts and the average transcript count of *Meg3* are decreased, whereas the percentage of cells expressing *Snhg18* is increased in fibrotic *Col14a1* matrix fibroblasts (Figure 4E). *Meg3* lncRNA has been suggested to be expressed in tissue fibrosis (He et al., 2014; Piccoli et al., 2017). The top discriminative extracellular expressing genes are *Pi16* and *Mmp3* for *Col14a1* matrix fibroblasts, but with low transcript levels. *Clec3b* and *Dcn* are more significantly expressed, but with less distinction (Figure 4F). For transcription factors, mesoderm homeobox gene *Prrx1* is the top factor in *Col14a1* matrix fibroblasts, with *Aebp1* and *Lbh* highly expressed as well (Figures 4G and 4H).

### Elucidation of a Lipofibroblast Gene Signature

Lipofibroblasts are lipid-containing interstitial fibroblasts (McGowan and Torday, 1997; Torday and Rehan, 2016). The previously suggested markers for lipofibroblasts include *Adrp* (El Agha et al., 2017; Schultz et al., 2002), *Pparg* (Varisco et al., 2012), *Fabp1*, *Fabp 4*, *Fabp5* (Chen et al., 1998, 2012; Li et al., 2016), and *Lpl* (Imamura et al., 2002). We found that these *Adrp* and *Pparg* highly expressing MCs were clustered together to form a distinct subpopulation, and at the same time, this cluster also expresses considerable levels of *Fabp1,4,5*, *Lpl*, and *Lipa*. Therefore, we referred to this cluster as lipofibroblasts (Figures 5A–5C). We further examined the cluster and found that this subtype expresses immune function-related genes along with mesenchymal genes. The top signature genes include *Ear1* and *Ear2*, *Mrc1*, *Ccl6*, *Plet1*, *Abcg1*, and *Krt79* (Figures 5D and 5E). Furthermore, the cluster also expresses common fibroblast genes such as *Pdgfra*, *Vim*, *Col4a1*, and *Fn1* (Figure S2A). Therefore, the expression patterns of the lipofibroblast subtype possessed a lipid synthesis and transport gene signature, as well as a mesenchymal feature. The top expressing lncRNA is AI504432, which is located on the opposite strand of the *Kcna3* gene, with expression level and percentage decreased in fibrotic lipofibroblasts (Figure 5F). We also compared the expression levels for the top 50 highest expressed genes, including extracellular and plasma membrane genes, between normal and fibrotic lipofibroblasts (Figure 5G). It is interesting that M2 macrophage-like signature genes (*Chil3*, *Mrc1*, *IL18*, and *CD9*) (Lechner et al., 2017), together with mesenchymal genes (*Mlc1*, *Plek*, *CD44*, *Ptpn12*, *and Slpi*), are expressed in the lipofibroblast subtype (Figures S2B and 5G). The most distinctive transcription factor for the lipofibroblast is *Nfib*, and its expression level is the lowest within the MC subtypes (Figure 5H). Other top expressed transcription factors include *Runx1*, *Baz1a*, *Cebpa*, and *Hcls1* (Figure 5I).

### Identification of a Subgroup of Potential Mesenchymal Progenitors

Mesenchymal progenitors are characterized by their self-renewal capacity and a signature enriched with proliferative genes. The term "mesenchymal progenitor" was adapted from the nomenclature by the LungGENS project "Proliferative Mesenchymal Progenitors" (Du et al., 2015). We observed a cluster of cells expressing high levels of *Top2a* and *Mki67*. We henceforth hypothesized that these cells could act as mesenchymal progenitors (Figures S3A–S3C). We further characterized the predominantly expressed genes within this cluster and found that *Hist1h2ap*, *Ube2c*, *H2afx*, *Cks2*, *Hmgb2*, and *Ccnb2* were distinct markers. These genes are related to cell cycle, cell proliferation, DNA metabolism, nuclear division, and mitotic cell cycle (Figures S3D and S3E). They are variably expressed during normal and fibrotic status but typically present in the mesenchymal progenitor cluster. Top expressed lncRNAs in this cluster were *Malat1* and *Lockd* (Figure S3F). The most significant extracellular expressed gene is *Hmgb2*. The distinct plasma membrane genes are *S100a8* and *Cd52*. Given the insufficiency of *S100a8* surface expression, CD52 would be a better cell surface marker for the mesenchymal progenitors (Figure S3G). In addition, *Hmgb2* is the most highly expressed transcription factor in the mesenchymal progenitor subtype (Figure S3H), together with *Ezh2*, *Uhrf1*, *Mcm6*, *Hmgb3*, and *Mcm5* as the specifically expressed transcription factors in mesenchymal progenitors (Figure S3I). The LungGENS project identified 453 signature genes for the proliferative mesenchymal progenitors (PMPs). These 453 genes showed up in our differentiated gene list for mesenchymal progenitors (both D0 and D21) (Table S1), with various p value ranks. Within the 23 genes that were upregulated and log2 fold change >2 in the D0 mesenchymal progenitors, 13 genes were identical as PMP signature genes. Forty-six genes are upregulated and log2 fold change >2 in the D21 mesenchymal progenitors, and 23 genes are the same as PMP signature genes (Table S2). The gene signatures of PMPs and mesenchymal progenitors are similar, regardless that PMPs were sampled from E16.5 mouse lung.

### Classification of Mesothelial Cells

Mesothelial cells provide a slippery, non-adhesive, and protective surface that wrap the internal organs and the body's cavities. WT1 lineage mesothelial cells were shown to give rise to desmin$^{+}$CD34$^{+}$ fibroblasts, as well as bronchial and vascular smooth muscle cells (Cano et al., 2013; Dixit et al., 2013). The previously reported markers for mesothelial cells are *Wt1*, *Upk3b*, *Lrrn4*, *Msln*, and *Calb2* (Du et al., 2015; Kanamori-Katayama et al., 2011; Que et al., 2008; Rinkevich et al., 2012). Notably, cells enriched for these common genes are clustered tightly, and we subsequently identified them as the mesothelial

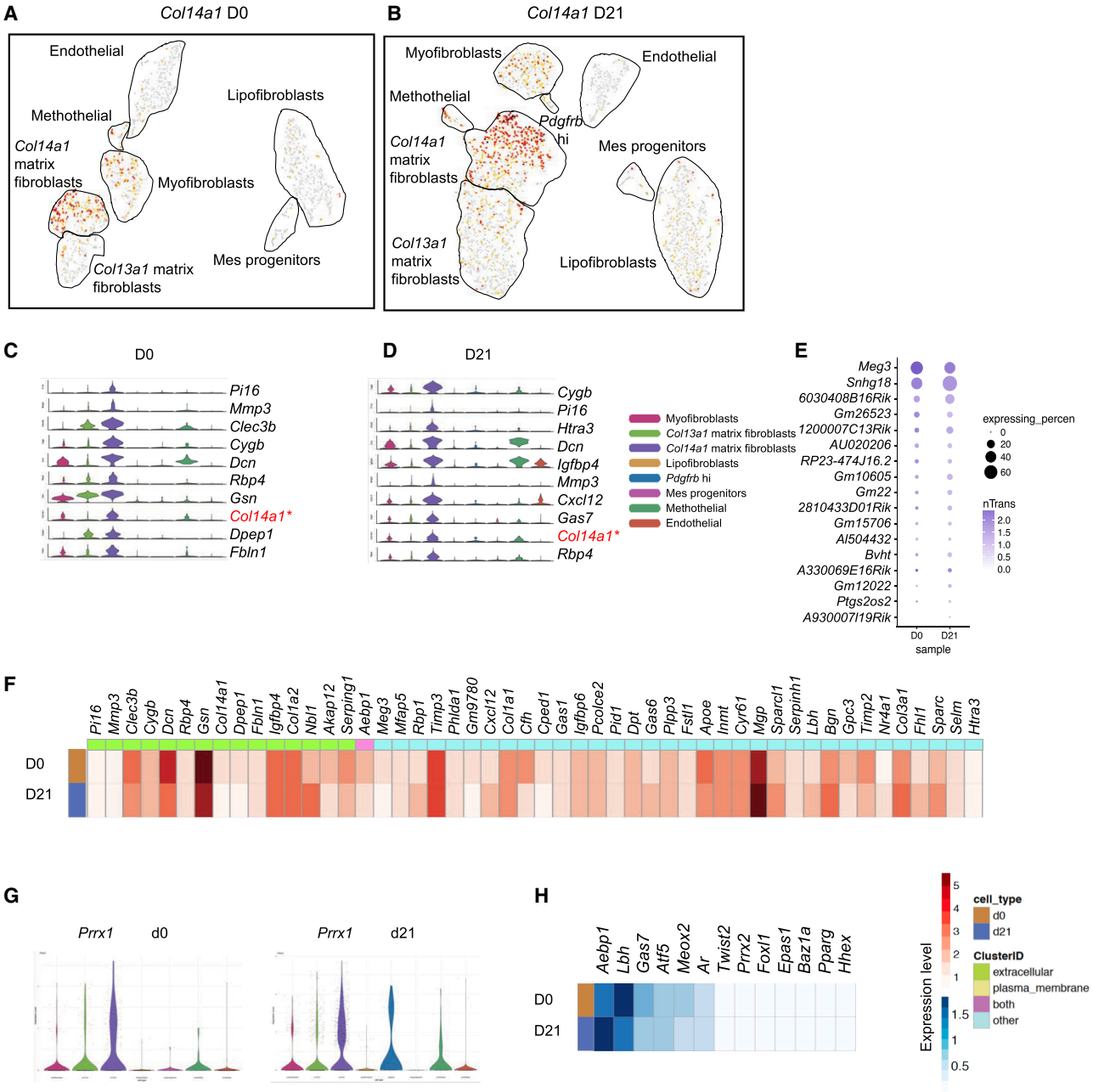


**Figure 4. Characterization of *Col14a1* Matrix Fibroblasts**

(A and B) *Col14a1* expression in normal (A) and fibrotic (B) MC subtypes projected by t-SNE.

(C and D) Enriched signature genes within the normal (C) and fibrotic (D) *Col14a1* MC subtype.

(E) Subtype significantly expressed lncRNAs.

(F) Significantly differentiated genes with the indication of cellular location enriched in the *Col14a1* subtype.

(G) *Prrx1* as the master transcription factor in the *Col14a1* subtype.

(H) Heatmap showing the highly distinct transcription factors.

cell subtype (Figures S4A–S4C). Identification of the subtype distinguished genes revealed *Lgals2*, *Cxcl13*, *Gpm6a*, *Rspo1*, and *Nkain4* as novel putative markers for mesothelial cells (Figures S4D and S4E). The top lncRNA for the mesothelial subtype is *Gm12840* (Figure S4F). The 50 most significant genes were highly and specifically expressed in mesothelial cells (Figure S4G). Zinc finger gene *Bnc1* is the best transcription factor uniquely identified in this cluster (Figure S4H). Other highly distinctive transcription factors include *Aebp1*, *Wt1*, *Gata6*, and *pdlim4* (Figure S4I).

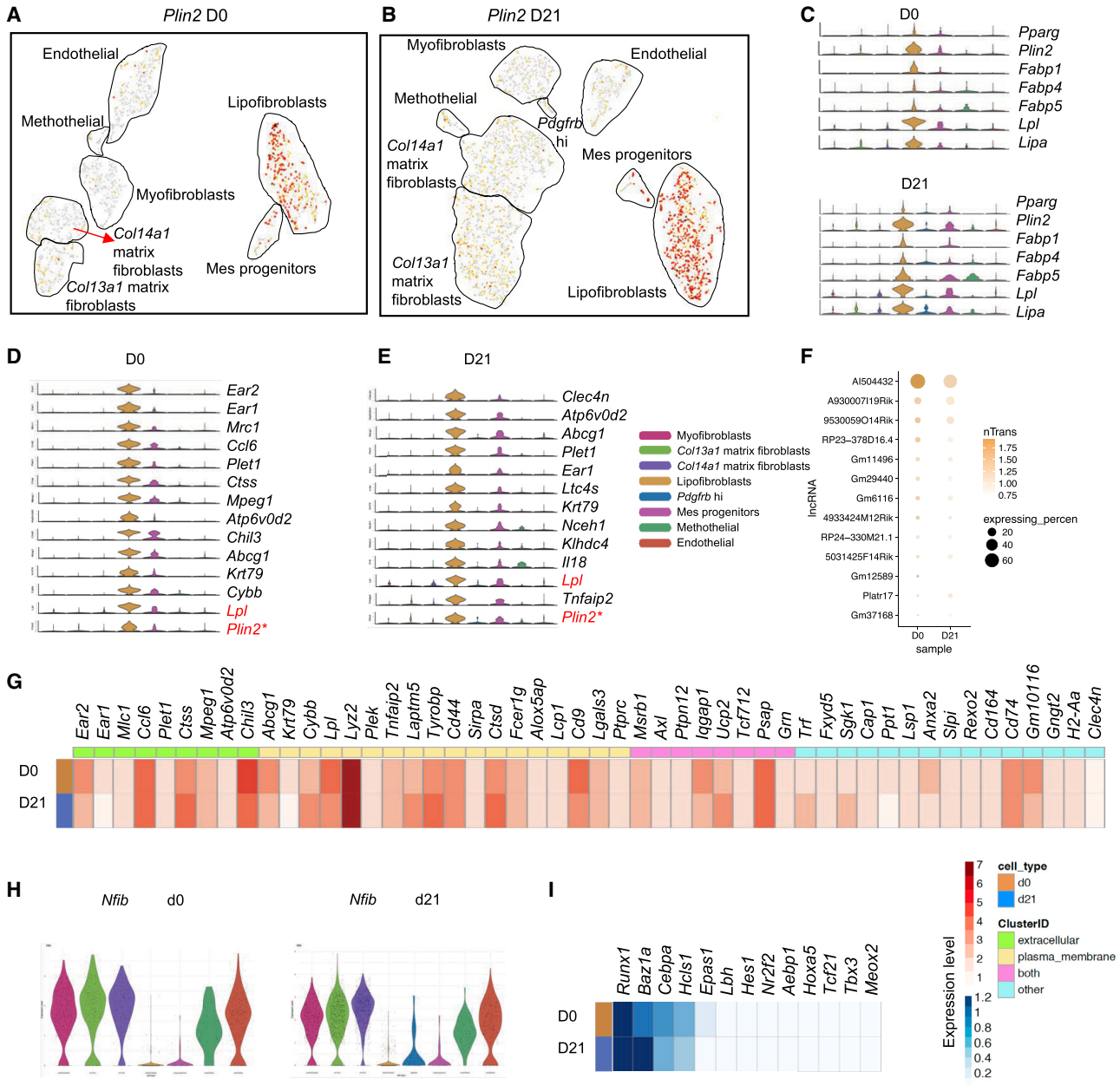


**Figure 5. Molecular Census of Lipofibroblasts**

(A and B) Signature gene *Plin2* expression was visualized in t-SNE plots of normal (A) and fibrotic (B) MCs.

(C) Violin plots of single-cell expression levels of known lipofibroblast genes across the MC subtypes.

(D and E) Top unique expressed genes in the normal (D) and fibrotic (E) lipofibroblast subtype.

(F) Expression patterns of lncRNAs in normal and fibrotic lipofibroblasts.

(G) Averaged expression of lipofibroblast significant genes in heatmap view. Genes were labeled with the cellular location, as indicated.

(H) *Nfib* as the most significantly lower expressed transcription factor across the MC subtypes.

(I) Top transcription factors shown in the lipofibroblast subtype.

## Discovering the Newly Emerging *Pdgfrb* High Fibroblasts in Fibrotic Lung

The comparison of normal and fibrotic MCs led us to uncover a newly emerging MC subtype expressing high levels of *Pdgfrb*. The *Pdgfrb* expressing cells were scattered in the myofibroblast, matrix fibroblast, mesothelial, and endothelial subtypes in normal MCs; the same pattern was found in fibrotic MCs, but the proportion of *Pdgfrb* expressing cells was increased. When using Pdgfrβ antibody to stain fibrotic lungs, the labeled cells were expanded as compared to normal lungs (Barron et al., 2016; Xie et al., 2016), which is consistent with our scRNA-seq data (Figure S5A). In addition, the *Pdgfrb* highly

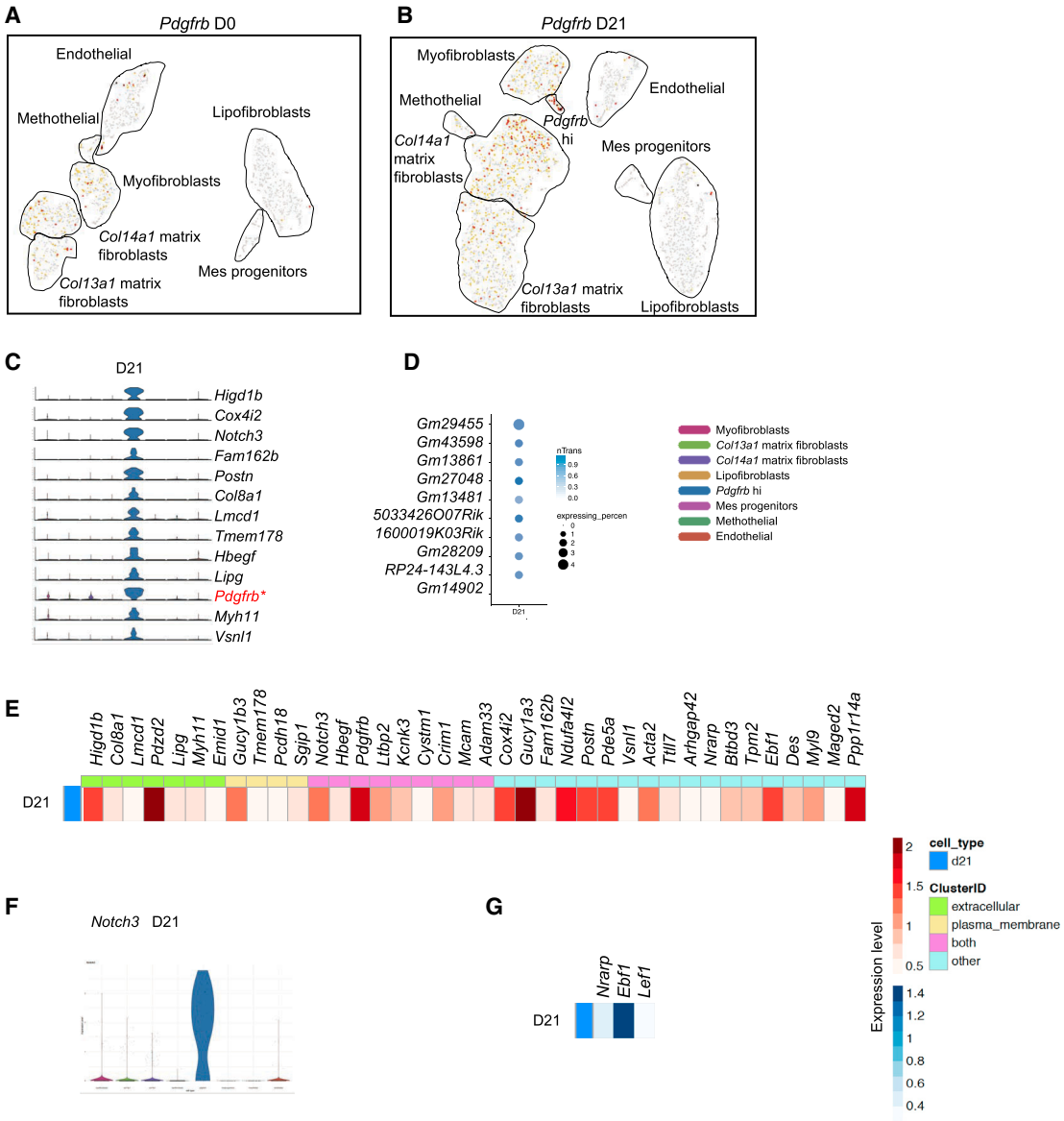


**Figure 6. Newly Emerging Fibrotic MC Subtype Expressing a High Level of *Pdgfrb***

(A and B) *Pdgfrb* expression in normal (A) and fibrotic (B) MC subtypes.

(C–G) Highly unique genes (C), lncRNAs (D), significantly expressed extracellular and plasma membrane expressing genes (E), top transcription factor (F), and enriched transcription factors (G) expressed in fibrotic *Pdgfrb* hi subtype.

expressing MCs were clustered together and can be distinguished collectively from the nearby myofibroblast subtype (Figures 6A and 6B). Thus, despite co-expressing genes such as *Acta2* and *Kcnk3*, *Pdgfrb* hi and myofibroblast subtypes were separated and represent distinct clusters. *Pdgfrb* hi fibroblasts expressed perfectly discriminating markers, including *Higd1b*, *Cox4i2*, *Notch3*, *Fam162b*, *Postn*, *Col8a1*, *Lmcd1*, *Tmem178*, *Hbegf*, and *Lipg* (Figure 6C). lncRNAs found in the *Pdgfrb* hi subtype were not remarkable (Figure 6D). *Postn*, *Higd1b*, and *Col8a1* were highly distinctive extracellular expressing genes. Plasma membrane expressing genes other than *Pdgfrb* were *Gucy1b3*, *Tmem178*, *Pcdh18*, and *Sgip1* (Figure 6E). The *Pdgfrb* hi subtype was best delineated by transcription factor *Notch3* (Figure 6F) and Notch downstream effector *Nrarp*. Other transcription factors such as *Ebf1* and *Lef1* were discriminatively expressed in this subtype (Figure 6G). It is interesting that Nrarp also is involved in stabilizing LEF1 in regulating Wnt signaling (Ishitani et al., 2005), suggesting a role of the Notch-Wnt signaling pathways in this *Pdgfrb* hi subtype. Because *Notch3* and *Pdgfrb* have been suggested to be pericyte markers, we checked the other previously suggested pericyte markers in the current scRNA-seq data: *Mcam* (*Cd146*) (Barron et al., 2016), labeled *Pdgfrb* hi, endothelial, lipofibroblast subtypes (Figure S5B); *Cspg4* (*Ng2*) (Barron et al., 2016; Hung et al.,

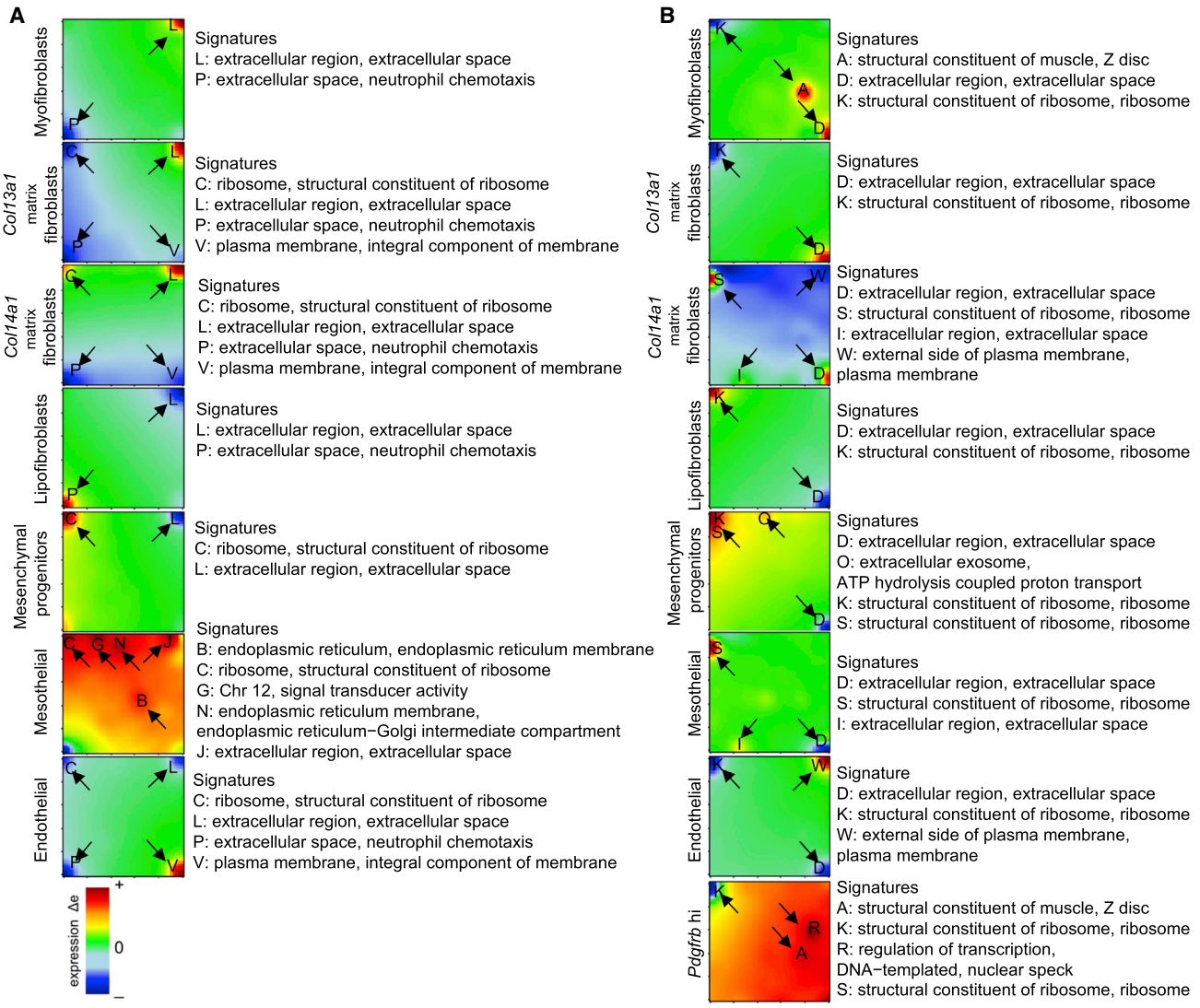


(legend on next page)

2013), labeled few cells scattered in the *Pdgfrb* hi, myofibroblast, matrix fibroblast; and lipofibroblast MC subtypes (Figure S5C). These data suggested that *Pdgfrb* hi fibroblasts are newly emerging MCs in response to the fibrotic injury, but there was no distinct pericyte cluster in the analysis. The potential overlaps with pericytes anatomically and functionally remain to be determined.

## Uncovering the Transcriptional Program of Endothelial Cells

Given the fact that a close relation exists between endothelial cells and fibroblasts (Kumar et al., 2014; Xie et al., 2016), we included endothelial cells in the analysis. We detected a cluster of cells enriched for endothelial cell markers, including *Pecam1*, *Cdh5*, *Edn1*, *Kdr*, *Ets1*, and *Gata2* (Figures S6A–S6D). A set of strong, unique signature genes, including *Cldn5*, *Cyyr1*, *Clic5*, *Clec14a*, and *Tspan7*, were found to be highly and specifically expressed in endothelial cells from both normal and fibrotic lungs (Figures S6E and S6F). *Bvht* is the top endothelial expressed lncRNA and the prevalence of this lncRNA in endothelial cluster is ~30% (Figure S6G). *Bvht* has been shown to have a key role in cardiac differentiation, including vascular endothelium (Klattenhoff et al., 2013). The top 50 most distinct signature genes in endothelial cells were plotted as a heatmap and analyzed for the differences between normal and fibrotic lungs (Figure S6H). The most uniquely discriminative transcription factor is *Sox18*, which is slightly increased in the endothelial cluster in fibrotic lungs (Figure S6I). Transcription factors, including *Epas1*, *Klf2*, *Ppp1r16*, *Gata2*, *Sox17*, and *Ahr*, also are significantly expressed in endothelial cells (Figure S6J).

## Differentiation Potential of the MC Subtypes

We used self-organizing maps (SOMs) by single-cell R analysis tool based on SOM machine learning (SCRAT) (Camp et al., 2017) to determine and envision coincidental gene sets exhibited in each population of MCs during fibrogenesis formation. The analysis revealed that MC subtypes expressed variable signatures under normal and fibrotic conditions (Figures 7A and 7B). We demonstrated multiple subtype-specific gene signatures, including extracellular region, extracellular space, neutrophil chemotaxis, ribosome, structural constituent of ribosomes, plasma membrane, integral component of membrane, endoplasmic reticulum, endoplasmic reticulum membrane, chromosome 12, signal transducer activity, structural constituent of muscle, ATP hydrolysis-coupled proton transport, regulation of transcription, and DNA-templated nuclear speck (Figures 7A and 7B). Notably, at the fibrotic stage, the myofibroblast subtype acquired a gene signature involving the structural constituent of muscle. *Col13a1* and *Col14a1* matrix fibroblasts as well as lipofibroblasts lost the signature of neutrophil chemotaxis. Mesothelial cells displayed gene signatures similar to *Col14a1* matrix fibroblasts following fibrotic injury.

We then projected MCs onto the SCRAT for sample similarity and pseudo-time analysis, which provides information inferring lineage trajectories from single-cell expression data in the form of 2D bifurcation. We assigned major MC subtypes onto SCRAT, including myofibroblasts, *Col13a1* matrix fibroblasts, *Col14a1* matrix fibroblasts, lipofibroblasts, mesenchymal progenitors, and *Pdgfrb* hi MCs. We found that the correlation-spanning tree and trajectory report displayed a directed hierarchical relation of the various subgroups, starting from mesenchymal progenitors and bifurcated to other MC subtypes (Figures 7C and 7D). It is interesting that our SCRAT analysis demonstrated a different lineage hierarchy among the MC subpopulations between normal and fibrotic stages. In the normal lung, mesenchymal progenitors bifurcated to lipofibroblasts and *Col14a1* matrix fibroblasts, whereas *Col14a1* matrix fibroblasts diverged to myofibroblasts and *Col13a1* matrix fibroblasts. In the fibrotic lung, mesenchymal progenitors branched to lipofibroblasts and then lineage differentiated to the *Pdgfrb* hi subtype, myofibroblasts, *Col14a1* matrix fibroblasts, and *Col13a1* matrix fibroblasts sequentially.

## Comparison between the Present Study and Recent Reports of Single-Cell Sequencing of Mesenchymal Cells

Recent single-cell studies reported by Zepp et al. (2017) showed that distinct Axin2$^+$Pdgfr$\alpha^+$ mesenchymal alveolar niche cell (MANC) and Axin2$^+$ mesenchymal progenitor (AMP) subpopulations are found by scRNA-seq. We extracted the significant genes of MANCs and AMPs from the reports of Zepp et al. (2017) and compared the transcriptional programs of these two subgroups with our study (Figures S7A and S7B). AMPs, which have higher Acta2 expression levels, show correlation with our myofibroblast subgroup on D0 and *Pdgfrb* hi subgroup on D21. MANCs, which are expanded post-injury and mainly Pdgfr$\alpha^+$, are similar to the Col13a1/Col14a1 matrix fibroblasts. Our analysis revealed two more mesenchymal cell types in the normal lung compared to the Zepp et al. (2017) study. This may be because the cells included in our study are a larger population. Our analysis included all of the Epcam$^-$CD31$^-$CD45$^-$ cells, and Tbx4 lineage cells represent ~90% of the total Epcam$^-$CD31$^-$CD45$^-$ cells (Xie et al., 2016). All of the Axin2$^+$, Axin2$^+$Pdgfr$\alpha^+$, Pdgfr$\alpha^+$, and other cells compose ~50% of the Epcam$^-$CD31$^-$CD45$^-$ cells, when interpreted from Figures S1H and S1I in Zepp et al. (2017). Wnt2$^+$ cells may constitute only a portion of the rest of the mesenchymal cells because Wnt2$^+$ cells have ~85% overlap with Pdgfr$\alpha^+$ cells and ~30% overlap with Axin2$^+$ cells. It is unexpected to see that the scRNA-seq analysis segregated Wnt2$^+$ cells so well from the other populations when they are supposed to have large overlaps. All of these in turn may lead this previous analysis to reveal limited mesenchymal subgroups.

A recent single-cell study by Lee et al. (2017) showed that Lgr5 and Lgr6 lineage cells are epithelial niche-promoting MCs

**Figure 7. Metagene Analysis and Differential Potential of MCs**

(A and B) Metagene profile for each MC subtype in normal status (A) and fibrotic status (B). Arrows mark overexpressed and underexpressed metagene signatures. Red shows overexpression and blue shows underexpression.

(C and D) Lineage bifurcation of five MC subtypes in normal (C) and fibrotic lung (D). Cells on the same or neighboring branches are expected to be more hierarchically related. Color coding indicates pseudo-time scores of the cells.

located in alveolar and airway compartments, respectively. In our study, most of the Lgr5 and Lgr6 expressing cells are found within Acta2 hi expressing myofibroblasts (Figure S7C). In the D0 single-cell analysis, there are 93 $Lgr5^+$ cells, 44 $Lgr6^+$ cells, 13 $Lgr5^+/Lgr6^+$ cells, and 19 $Lgr6^+/Acta2^+$ cells. By D21, there are 124 $Lgr5^+$ cells, 120 $Lgr6^+$ cells, 31 $Lgr5^+/Lgr6^+$ cells, and 71 $Lgr6^+/Acta2^+$ cells. Lgr5 and Lgr6 may be the two subclusters of the myofibroblast subgroup with distinct locations. The $Lgr5^+/Lgr6^+$ cells found in our analysis are consistent with the claim by Lee et al. (2017) that Lgr6 marks cell populations expressing Lgr5.

## DISCUSSION

In this study, we used unbiased single-cell transcriptome analyses to comprehensively classify the MC subtypes and cell lineage potential of individual MCs in the normal and fibrotic mouse lung. The analyses identified adult pulmonary MCs, including myofibroblasts, *Col13a1* matrix fibroblasts, *Col14a1* matrix fibroblasts, lipofibroblasts, mesenchymal progenitors, and mesothelial cells, as heterogeneous populations. In addition, the *Pdgfrb* hi fibroblast subpopulation was found to emerge in fibrogenesis. Our data provided combinatorial information of the signature genes, lncRNAs, extracellular and plasma membrane genes, and transcription factors for each of the MC subtypes. The fibroblast differentiation potential analyses identified different cell lineage trajectories between normal homeostasis and fibrotic conditions.

### Are Myofibroblasts the Major Expanded MCs in Fibrotic Lung?

Myofibroblasts express αSMA with features reminiscent of both fibroblasts and smooth muscle cells (Hinz et al., 2007), and are the vital players in fibrotic diseases (Wynn and Ramalingam, 2012). When performing αSMA antibody staining or using *αSMA-GFP*-reporting mice, $\alpha SMA^+$ cells are dramatically expanded during fibrogenesis (Xie et al., 2016). We observed that *Acta2* highly expressing cells are within the myofibroblast subtype; the low *Acta2*-expressing cells that express *Col1a1* are matrix fibroblast subtypes. The percentage of matrix fibroblasts is ~30% in normal MCs and increases to 50% in the fibrotic MCs. These scRNA-seq analyses suggest that αSMA is not specific enough to discriminate myofibroblasts from matrix fibroblasts. Therefore, many previously reported data that αSMA-expressing cells expand in lung fibrosis may be in fact mainly the result of matrix fibroblast amplification.

### Lipofibroblasts Are Further Delineated under Homeostatic and Fibrotic Conditions

Lipofibroblasts contain lipid in the form of large cytoplasmic lipid droplets without a limiting biomembrane or lipid vacuoles (McGowan and Torday, 1997; Tahedl et al., 2014). Lipofibroblasts are involved in alveolar development and regeneration associated with alveolar epithelial type II cells (AECII) surfactant synthesis and vitamin A (retinoic acid) storage (Tahedl et al., 2014), and contribute to the AECII stem cell niche in the adult mouse lung (Barkauskas et al., 2013). Adipose differentiation-related protein (ADRP, encoded by *Plin2*) is believed to be the major component that mediates the consumption of lipid inclusions in lipofibroblasts and their subsequent transport to AECII cells (Friedmacher et al., 2014). Common adipocyte genes, including *Pparg*, *Plin2*, *Fabp1*, *Fabp4*, *Fabp5*, *Lpl*, and *Lipa*, are featured in lipofibroblasts (Chen et al., 1998, 2012; El Agha et al., 2017; Imamura et al., 2002; Li et al., 2016; Schultz et al., 2002; Varisco et al., 2012). On the basis of these previously suggested lipofibroblast markers, we identified the lipofibroblast subtype in which these markers are substantially highly expressed in our scRNA-seq data. These cells also express common fibroblast markers such as *Vim*, *Col4a1*, and *Fn1*. Concurrently, this subtype may exhibit signature genes related to immune responses. Specifically, an M2-like macrophage gene signature also was found in the subtype. However, lipofibroblasts do not express classical macrophage markers such as *Ccr2*, *Lst1*, *Ms4a6c*, *plac8*, and *Ifitm3*. These M2-like signature genes include *Chil3*, *Mrc1(CD206)*, *IL18*, and *CD9*. A recent study showed that a subset of M2-like macrophages was defined by using scRNA-seq of FACS-sorted 68 $CD45^+$, $CSF1R^-GFP^+$, $F4/80^+$, and $Ly6G^-$ individual cells from mouse lung 7 days post-partial pneumonectomy and was a component of the regenerative AECII niche (Lechner et al., 2017). The relation between lipofibroblasts and M2-like macrophages warrants further investigation.

### Are Lipofibroblasts *Pdgfra*$^+$ Cells?

It is reported that Pdgfrα was expressed in a population of stem cell antigen-1 $(Sca1)^+$ and $CD34^+$, $CD45^-$, $CD31^-$, and $Thy\text{-}1^+$ cells, which also were lipid-staining positive (McQualter et al., 2009), $Pdgfra^+$ cells from *Pdgfra*;H2B-GFP mice contained lipid droplets and were supportive of the expansion and differentiation of epithelial cells *in vitro* (Barkauskas et al., 2013). A subpopulation of $Pdgfr\alpha^+$ fibroblasts are $\alpha SMA^+$ peribronchiolar smooth muscle and myofibroblasts in alveolar development (Chen et al., 2012; Endale et al., 2017). By using *Pdgfra*-GFP mice, Pdgfrα expressing precursor cells differentiate into myofibroblasts as well as lipofibroblasts, while the constitutive *Pdgfra-cre* mice revealed that the Pdgfrα signaling is restricted to bronchial smooth muscle cells and alveolar fibroblasts. Therefore, the overlap and the differences between $Pdgfr\alpha^+$ fibroblasts and lipofibroblasts can be delineated. It is interesting that our scRNA-seq data showed that $Pdgfra^+$ cells were mainly within *Col13a1* and *Col14a1* matrix fibroblasts. *Pdgfra* expression was low in $Acta2^+$ myofibroblasts and lipofibroblasts (Figure S2B). Some $Pdgfra^+$ matrix fibroblasts expressed *Adrp*, *Lpl*, and *Lipa*, but not *Pparg* and *Fabp1,4,5*. These results provide new insights into $Pdgfra^+$ cells and suggest that they are mainly matrix fibroblasts and can be transdifferentiated from lipofibroblasts.

### Are the Newly Emerging *Pdgfrb* Hi Cells during Fibrogenesis Pericytes?

Our scRNA-seq observations suggested that the *Pdgfrb* hi subtype is a newly emerging MC population in response to the fibrotic injury. Pericytes were reported to be marked by Pdgfrβ protein expression and have established their interactions with endothelial cells (Barron et al., 2016). When we used Pdgfrβ antibody to stain fibrotic lungs, the labeled cells were expanded compared to normal lungs (Barron et al., 2016; Xie et al.,

2016). By analyzing the expression of pericyte markers (*Pdgfrb*, *Mcam*, and *Cspg4*), our scRNA-seq data did not indicate a unique cluster for pericytes but suggested a phenomenon that pericytes are heterogeneous and plastic populations (Barron et al., 2016) and that they are overlapping with myofibroblasts and matrix fibroblasts. The newly emerging *Pdgfrb* hi MC subtype has uniquely expressed genes that can be cleanly separated from other MCs.

### Mesothelial Cells Contribute to Mesenchyme Expansion

Mesothelium contributes to lung mesenchyme during lung development (Que et al., 2008). Wt-1 lineage-traced mesothelium gives rise to interstitial fibroblasts and myofibroblasts, which reside outside the blood vessels and alveoli in the embryonic lung (Que et al., 2008). The contribution of mesothelium to mesenchyme also was detected in disease contexts, including peritoneal, liver, and lung fibrosis (Li et al., 2013; Lua et al., 2015; von Gise et al., 2016). In addition, mesothelial cells can be lineage traced by mesenchymal transcription factor Tbx4 in the lung (Kumar et al., 2014; Xie et al., 2016). Our scRNA-seq data demonstrated well-clustered mesothelial cells in total MCs and in $tdT^{+}GFP^{+}$ cells from $\alpha$*SMA*-GFP;*Tbx4-Cre;Rosa26-tdTomato* mice. Analyses of SOM gene sets revealed that the mesothelial cells displayed gene signatures similar to *Col14a1* matrix fibroblasts in fibrotic lung. Significant gene and transcription factor analyses confirmed previously identified mesothelial markers. Thus, our data confirmed that mesothelial cells contribute to mesenchyme expansion.

### Regulation of Fibroblast Subtypes by lncRNAs

lncRNAs are emerging as valuable mediators for fibrotic disease (Thum, 2014; Tzouvelekis and Kaminski, 2015). Notably, *Malat1* is highly expressed in the myofibroblast and mesenchymal progenitor subtype. *MALAT1* is one of the top expressed lncRNAs in patients with nonalcoholic steatohepatitis fibrosis. Its expression was increased in activated hepatic stellate cells (Leti et al., 2017). *Neat1* is the most abundantly expressed lncRNA in *Col13a1* matrix fibroblasts. It was reported that *Neat1* expression was significantly elevated in mouse liver fibrosis and activated hepatic stellate cells. Suppression of *Neat1* decreased liver fibrosis (Yu et al., 2017). Furthermore, *Meg3* is the most distinctly expressed lncRNA in *Col14a1* matrix fibroblasts, and its expression was decreased upon fibrotic injury. It is interesting that *Meg3* has been reported to be the highest expressed lncRNA found in cardiac fibroblasts by global lncRNA profiling, and its inhibition *in vivo* decreased cardiac fibrosis. Silencing of *Meg3* in cardiac fibroblasts decreased cardiac fibrosis (Piccoli et al., 2017). Thus, exploration of these distinguished lncRNAs in different mesenchymal subtypes will provide new insights into fibrogenesis.

### Conceptual Exploration of Subgroup Trajectory

The trajectory analysis has been used to delineate the cell lineage differentiation in developmental or disease conditions (Savage et al., 2017; Yan et al., 2017). Pseudo-time analysis implies the state of the lineage initiation subgroup and the potential capacity of transdifferentiation of each subgroup. Cells located on the same or adjacent branches are expected to be more hierarchically related compared to cells on the neighboring branches in a given trajectory tree.

The mesenchymal progenitors are the lineage-initiation MC subgroup in both normal and fibrotic lung. The demonstration that mesenchymal progenitors have the capacity to reconstitute an entire mesenchymal trajectory tree suggested a similarity between the mesenchymal progenitors and previously reported mesenchymal stem cells, although the differences between the two cell types cannot be ignored. Mesenchymal stem cells were reported to be able to differentiate into multiple cell types, including fibroblasts, adipocytes, osteoblasts, chondrocytes, myocytes, and neurons. Our scRNA-seq analysis defined mesenchymal progenitors as resident lung cells. A trajectory analysis found that these progenitors could directly differentiate into lipofibroblasts and *Col14a1* matrix fibroblasts. Our trajectory analysis also suggested that lipofibroblasts are poised for commitment to myofibroblasts through *Pdgfrb* hi subgroup in fibrotic lungs. This prediction is well correlated with a recent report that lipogenic fibroblasts or lipofibroblasts are a source of activated myofibroblasts in lung fibrosis (El Agha et al., 2017).

Experimental and biological characterizations such as precise lineage tracing and transcriptional conversion of mesenchymal progenitors (and mesenchymal subgroups) and the potential hierarchical differentiation in normal and in disease conditions warrant further investigation. Nevertheless, our trajectory analysis is inconsistent with previous reports and is our attempt to provide a conceptual framework to unmask the hierarchical relations between the mesenchymal subgroups.

In summary, the single-cell transcriptomic analyses dissected heterogeneous MC subtypes in both normal adult and fibrotic mouse lung. These comprehensive analyses provide transcription profiles for delineating mesenchymal taxonomy and add significantly to our understanding of fibroblast subpopulations in lung health and disease by providing a new toolbox to explore effector functions in disease. The study revealed distinctive molecular signatures for mesenchymal subsets in the lung, providing a foundation to augment our understanding of fibroblast subpopulations and to identify cell markers at the protein level, localization in the lung, signaling programs, and future functional significance. Further identification of "pathogenic" fibroblast subpopulations in lung fibrosis will enable us to develop therapeutic targets, as well as more precise cellular and animal models for patients with progressive pulmonary fibrosis.

## EXPERIMENTAL PROCEDURES

### Mice

Triple-heterozygous $\alpha$*SMA*-GFP;*Tbx4-Cre;Rosa26-tdTomato* mice were used. All of the mice were on a C57BL/6 background. The mouse studies were approved by the Institutional Animal Care and Use Committee at Cedars-Sinai Medical Center (protocols IACUC004722 and IACUC004751).

### Sequencing Library Construction Using the 10x Genomics Chromium Platform

scRNA-seq libraries were prepared per the Single Cell 3′ Reagent Kit User Guide v2 (10x Genomics). Cellular suspensions were loaded on a Chromium Controller instrument (10x Genomics) to generate single-cell gel bead-in-emulsions (GEMs). GEM-reverse transcriptions (GEM-RTs) were performed in a Veriti 96-well thermal cycler (Thermo Fisher Scientific). After RT, GEMs

were harvested and the cDNAs were amplified and cleaned up with the SPRIselect Reagent Kit (Beckman Coulter). Indexed sequencing libraries were constructed using the Chromium Single-Cell 3′ Library Kit (10x Genomics) for enzymatic fragmentation, end-repair, A-tailing, adaptor ligation, ligation cleanup, sample index PCR, and PCR cleanup. The barcoded sequencing libraries were quantified by quantitative PCR using the KAPA Library Quantification Kit (KAPA Biosystems). Sequencing libraries were loaded on a NextSeq500 (Illumina) with a custom sequencing setting (26 bp for read 1 and 98 bp for read 2) to obtain a sequencing depth of ~80,000 reads per cell.

### Statistical Method

We used Cell Ranger version 1.3.1 (10x Genomics) to process raw sequencing data and Cell Ranger R kit version 2.0.0 and Seurat suite version 2.0.0 (Butler and Satija, 2017; Macosko et al., 2015) for downstream analysis. For clustering, principal-component analysis was performed for dimension reduction. Top 10 principal components (PCs) were selected by using a permutation-based test implemented in Seurat and passed to t-SNE for clustering visualization. sSeq version 1.0.0 integrated in the Cell Ranger R kit was used for modeling the gene expression with negative binomial distribution to identify genes whose expression was enriched in specific clusters. The Benjamini-Hochberg procedure was used for correcting errors of multiple testing.

## DATA AND SOFTWARE AVAILABILITY

The accession number for the raw data files of the RNA-seq analyses reported in this paper is GEO: GSE104154.

## SUPPLEMENTAL INFORMATION

Supplemental Information includes Supplemental Experimental Procedures, seven figures, and two tables and can be found with this article online at https://doi.org/10.1016/j.celrep.2018.03.010.

## ACKNOWLEDGMENTS

This study was supported by NIH grants P01 HL108793, R01 HL060539 (to P.W.N.), and R01 HL122068 (to D.J.). The authors would like to acknowledge Nargess Hassanzadeh-Kiabi and Andres Lopez at the Flow Cytometry Core of Cedars-Sinai Medical Center in Los Angeles for their assistance with FACS. The authors also are grateful for the assistance provided by Chintda Santiskulvong at Genomics Core of Cedars-Sinai Medical Center for single-cell RNA sequencing.

## AUTHOR CONTRIBUTIONS

Conceptualization, T.X., P.W.N. and D.J.; Software, Y.W. and N.D.; Validation and Formal Analysis, T.X., Y.W., and N.D.; RNA-seq Experiments, T.X. and N.L.; Investigation, G.H., F.T., V.K., N.L., Y.G., Y.W., N.D., Z.L., C.Y., P.C., B.S., J.L., T.X., and D.J.; Writing – Original Draft, T.X.; Writing – Review & Editing, Y.W., J.T., D.J., and P.W.N.; Funding Acquisition, D.J. and P.W.N.

## DECLARATION OF INTERESTS

The authors declare no competing interests

Received: November 2, 2017
Revised: February 23, 2018
Accepted: March 1, 2018
Published: March 27, 2018

## REFERENCES

Andreucci, J.J., Grant, D., Cox, D.M., Tomc, L.K., Prywes, R., Goldhamer, D.J., Rodrigues, N., Bédard, P.A., and McDermott, J.C. (2002). Composition and function of AP-1 transcription complexes during muscle cell differentiation. J. Biol. Chem. *277*, 16426–16432.

Bagchi, R.A., Roche, P., Aroutiounova, N., Espira, L., Abrenica, B., Schweitzer, R., and Czubryt, M.P. (2016). The transcription factor scleraxis is a critical regulator of cardiac fibroblast phenotype. BMC Biol. *14*, 21.

Barkauskas, C.E., Cronce, M.J., Rackley, C.R., Bowie, E.J., Keene, D.R., Stripp, B.R., Randell, S.H., Noble, P.W., and Hogan, B.L. (2013). Type 2 alveolar cells are stem cells in adult lung. J. Clin. Invest. *123*, 3025–3036.

Barron, L., Gharib, S.A., and Duffield, J.S. (2016). Lung pericytes and resident fibroblasts: busy multitaskers. Am. J. Pathol. *186*, 2519–2531.

Bochaton-Piallat, M.L., Gabbiani, G., and Hinz, B. (2016). The myofibroblast in wound healing and fibrosis: answered and unanswered questions. F1000Res. Published online April 26, 2016. https://doi.org/10.12688/f1000research.8190.1.

Butler, A., and Satija, R. (2017). Integrated analysis of single cell transcriptomic data across conditions, technologies, and species. bioRxiv, https://doi.org/10.1101/164889.

Camp, J.G., Sekine, K., Gerber, T., Loeffler-Wirth, H., Binder, H., Gac, M., Kanton, S., Kageyama, J., Damm, G., Seehofer, D., et al. (2017). Multilineage communication regulates human liver bud development from pluripotency. Nature *546*, 533–538.

Cano, E., Carmona, R., and Muñoz-Chápuli, R. (2013). Wt1-expressing progenitors contribute to multiple tissues in the developing lung. Am. J. Physiol. Lung Cell. Mol. Physiol. *305*, L322–L332.

Chen, H., Jackson, S., Doro, M., and McGowan, S. (1998). Perinatal expression of genes that may participate in lipid metabolism by lipid-laden lung fibroblasts. J. Lipid Res. *39*, 2483–2492.

Chen, L., Acciani, T., Le Cras, T., Lutzko, C., and Perl, A.K. (2012). Dynamic regulation of platelet-derived growth factor receptor $\alpha$ expression in alveolar fibroblasts during realveolarization. Am. J. Respir. Cell Mol. Biol. *47*, 517–527.

Derdak, S., Penney, D.P., Keng, P., Felch, M.E., Brown, D., and Phipps, R.P. (1992). Differential collagen and fibronectin production by Thy 1+ and Thy 1- lung fibroblast subpopulations. Am. J. Physiol. *263*, L283–L290.

Dixit, R., Ai, X., and Fine, A. (2013). Derivation of lung mesenchymal lineages from the fetal mesothelium requires hedgehog signaling for mesothelial cell entry. Development *140*, 4398–4406.

Du, Y., Guo, M., Whitsett, J.A., and Xu, Y. (2015). 'LungGENS': a web-based tool for mapping single-cell gene expression in the developing lung. Thorax *70*, 1092–1094.

El Agha, E., Al Alam, D., Carraro, G., MacKenzie, B., Goth, K., De Langhe, S.P., Voswinckel, R., Hajihosseini, M.K., Rehan, V.K., and Bellusci, S. (2012). Characterization of a novel fibroblast growth factor 10 (Fgf10) knock-in mouse line to target mesenchymal progenitors during embryonic development. PLoS One *7*, e38452.

El Agha, E., Moiseenko, A., Kheirollahi, V., De Langhe, S., Crnkovic, S., Kwapiszewska, G., Kosanovic, D., Schwind, F., Schermuly, R.T., Henneke, I., et al. (2017). Two-way conversion between lipogenic and myogenic fibroblastic phenotypes marks the progression and resolution of lung fibrosis. Cell Stem Cell *20*, 261–273e3.

Endale, M., Ahlfeld, S., Bao, E., Chen, X., Green, J., Bess, Z., Weirauch, M.T., Xu, Y., and Perl, A.K. (2017). Temporal, spatial, and phenotypical changes of PDGFR$\alpha$ expressing fibroblasts during late lung development. Dev. Biol. *425*, 161–175.

Friedmacher, F., Fujiwara, N., Hofmann, A.D., Takahashi, H., Alvarez, L.A., Gosemann, J.H., and Puri, P. (2014). Prenatal retinoic acid increases lipofibroblast expression in hypoplastic rat lungs with experimental congenital diaphragmatic hernia. J. Pediatr. Surg. *49*, 876–881.

Gurtner, G.C., Werner, S., Barrandon, Y., and Longaker, M.T. (2008). Wound repair and regeneration. Nature *453*, 314–321.

He, Y., Wu, Y.T., Huang, C., Meng, X.M., Ma, T.T., Wu, B.M., Xu, F.Y., Zhang, L., Lv, X.W., and Li, J. (2014). Inhibitory effects of long noncoding RNA MEG3 on hepatic stellate cells activation and liver fibrogenesis. Biochim. Biophys. Acta *1842*, 2204–2215.

Hinz, B., Phan, S.H., Thannickal, V.J., Galli, A., Bochaton-Piallat, M.L., and Gabbiani, G. (2007). The myofibroblast: one function, multiple origins. Am. J. Pathol. *170*, 1807–1816.

Hsia, L.T., Ashley, N., Ouaret, D., Wang, L.M., Wilding, J., and Bodmer, W.F. (2016). Myofibroblasts are distinguished from activated skin fibroblasts by the expression of AOC3 and other associated markers. Proc. Natl. Acad. Sci. USA *113*, E2162–E2171.

Hung, C., Linn, G., Chow, Y.H., Kobayashi, A., Mittelsteadt, K., Altemeier, W.A., Gharib, S.A., Schnapp, L.M., and Duffield, J.S. (2013). Role of lung pericytes and resident fibroblasts in the pathogenesis of pulmonary fibrosis. Am. J. Respir. Crit. Care Med. *188*, 820–830.

Imamura, M., Inoguchi, T., Ikuyama, S., Taniguchi, S., Kobayashi, K., Nakashima, N., and Nawata, H. (2002). ADRP stimulates lipid accumulation and lipid droplet formation in murine fibroblasts. Am. J. Physiol. Endocrinol. Metab. *283*, E775–E783.

Ishitani, T., Matsumoto, K., Chitnis, A.B., and Itoh, M. (2005). Nrarp functions to modulate neural-crest-cell differentiation by regulating LEF1 protein stability. Nat. Cell Biol. *7*, 1106–1112.

Jordana, M., Schulman, J., McSharry, C., Irving, L.B., Newhouse, M.T., Jordana, G., and Gauldie, J. (1988). Heterogeneous proliferative characteristics of human adult lung fibroblast lines and clonally derived fibroblasts from control and fibrotic tissue. Am. Rev. Respir. Dis. *137*, 579–584.

Kanamori-Katayama, M., Kaiho, A., Ishizu, Y., Okamura-Oho, Y., Hino, O., Abe, M., Kishimoto, T., Sekihara, H., Nakamura, Y., Suzuki, H., et al. (2011). LRRN4 and UPK3B are markers of primary mesothelial cells. PLoS ONE *6*, e25391.

Kimani, P.W., Holmes, A.J., Grossmann, R.E., and McGowan, S.E. (2009). PDGF-Ralpha gene expression predicts proliferation, but PDGF-A suppresses transdifferentiation of neonatal mouse lung myofibroblasts. Respir. Res. *10*, 119.

Klattenhoff, C.A., Scheuermann, J.C., Surface, L.E., Bradley, R.K., Fields, P.A., Steinhauser, M.L., Ding, H., Butty, V.L., Torrey, L., Haas, S., et al. (2013). Braveheart, a long noncoding RNA required for cardiovascular lineage commitment. Cell *152*, 570–583.

Kotaru, C., Schoonover, K.J., Trudeau, J.B., Huynh, M.L., Zhou, X., Hu, H., and Wenzel, S.E. (2006). Regional fibroblast heterogeneity in the lung: implications for remodeling. Am. J. Respir. Crit. Care Med. *173*, 1208–1215.

Kumar, M.E., Bogard, P.E., Espinoza, F.H., Menke, D.B., Kingsley, D.M., and Krasnow, M.A. (2014). Mesenchymal cells. Defining a mesenchymal progenitor niche at single-cell resolution. Science *346*, 1258810.

Lao, T., Jiang, Z., Yun, J., Qiu, W., Guo, F., Huang, C., Mancini, J.D., Gupta, K., Laucho-Contreras, M.E., Naing, Z.Z., et al. (2016). Hhip haploinsufficiency sensitizes mice to age-related emphysema. Proc. Natl. Acad. Sci. USA *113*, E4681–E4687.

Lechner, A.J., Driver, I.H., Lee, J., Conroy, C.M., Nagle, A., Locksley, R.M., and Rock, J.R. (2017). Recruited monocytes and type 2 immunity promote lung regeneration following pneumonectomy. Cell Stem Cell *21*, 120–134.e7.

Lee, J.H., Tammela, T., Hofree, M., Choi, J., Marjanovic, N.D., Han, S., Canner, D., Wu, K., Paschini, M., Bhang, D.H., et al. (2017). Anatomically and functionally distinct lung mesenchymal populations marked by Lgr5 and Lgr6. Cell *170*, 1149–1163.e12.

Leng, D., Huan, C., Xie, T., Liang, J., Wang, J., Dai, H., Wang, C., and Jiang, D. (2013). Meta-analysis of genetic programs between idiopathic pulmonary fibrosis and sarcoidosis. PLoS One *8*, e71059.

Leti, F., Legendre, C., Still, C.D., Chu, X., Petrick, A., Gerhard, G.S., and DiStefano, J.K. (2017). Altered expression of MALAT1 lncRNA in nonalcoholic steatohepatitis fibrosis regulates CXCL5 in hepatic stellate cells. Transl. Res. *190*, 25–39.e21.

Li, Y., Jiang, D., Liang, J., Meltzer, E.B., Gray, A., Miura, R., Wogensen, L., Yamaguchi, Y., and Noble, P.W. (2011). Severe lung fibrosis requires an invasive fibroblast phenotype regulated by hyaluronan and CD44. J. Exp. Med. *208*, 1459–1471.

Li, Y., Wang, J., and Asahina, K. (2013). Mesothelial cells give rise to hepatic stellate cells and myofibroblasts via mesothelial-mesenchymal transition in liver injury. Proc. Natl. Acad. Sci. USA *110*, 2324–2329.

Li, A., Ma, S., Smith, S.M., Lee, M.K., Fischer, A., Borok, Z., Bellusci, S., Li, C., and Minoo, P. (2016). Mesodermal ALK5 controls lung myofibroblast versus lipofibroblast cell fate. BMC Biol. *14*, 19.

Liang, J., Zhang, Y., Xie, T., Liu, N., Chen, H., Geng, Y., Kurkciyan, A., Mena, J.M., Stripp, B.R., Jiang, D., and Noble, P.W. (2016). Hyaluronan and TLR4 promote surfactant-protein-C-positive alveolar progenitor cell renewal and prevent severe pulmonary fibrosis in mice. Nat. Med. *22*, 1285–1293.

Liu, C., Gersch, R.P., Hawke, T.J., and Hadjiargyrou, M. (2010). Silencing of Mustn1 inhibits myogenic fusion and differentiation. Am. J. Physiol. Cell Physiol. *298*, C1100–C1108.

Lua, I., Li, Y., Pappoe, L.S., and Asahina, K. (2015). Myofibroblastic conversion and regeneration of mesothelial cells in peritoneal and liver fibrosis. Am. J. Pathol. *185*, 3258–3273.

Macosko, E.Z., Basu, A., Satija, R., Nemesh, J., Shekhar, K., Goldman, M., Tirosh, I., Bialas, A.R., Kamitaki, N., Martersteck, E.M., et al. (2015). Highly parallel genome-wide expression profiling of individual cells using nanoliter droplets. Cell *161*, 1202–1214.

McGowan, S.E., and Torday, J.S. (1997). The pulmonary lipofibroblast (lipid interstitial cell) and its contributions to alveolar development. Annu. Rev. Physiol. *59*, 43–62.

McQualter, J.L., Brouard, N., Williams, B., Baird, B.N., Sims-Lucas, S., Yuen, K., Nilsson, S.K., Simmons, P.J., and Bertoncello, I. (2009). Endogenous fibroblastic progenitor cells in the adult mouse lung are highly enriched in the sca-1 positive cell fraction. Stem Cells *27*, 623–633.

Piccoli, M.T., Gupta, S.K., Viereck, J., Foinquinos, A., Samolovac, S., Kramer, F.L., Garg, A., Remke, J., Zimmer, K., Batkai, S., and Thum, T. (2017). Inhibition of the cardiac fibroblast-enriched lncRNA*Meg3* prevents cardiac fibrosis and diastolic dysfunction. Circ. Res. *121*, 575–583.

Que, J., Wilm, B., Hasegawa, H., Wang, F., Bader, D., and Hogan, B.L. (2008). Mesothelium contributes to vascular smooth muscle and mesenchyme during lung development. Proc. Natl. Acad. Sci. USA *105*, 16626–16630.

Rinkevich, Y., Mori, T., Sahoo, D., Xu, P.X., Bermingham, J.R., Jr., and Weissman, I.L. (2012). Identification and prospective isolation of a mesothelial precursor lineage giving rise to smooth muscle cells and fibroblasts for mammalian internal organs, and their vasculature. Nat. Cell Biol. *14*, 1251–1260.

Robin, Y.M., Penel, N., Pérot, G., Neuville, A., Vélasco, V., Ranchère-Vince, D., Terrier, P., and Coindre, J.M. (2013). Transgelin is a novel marker of smooth muscle differentiation that improves diagnostic accuracy of leiomyosarcomas: a comparative immunohistochemical reappraisal of myogenic markers in 900 soft tissue tumors. Mod. Pathol. *26*, 502–510.

Rock, J.R., Barkauskas, C.E., Cronce, M.J., Xue, Y., Harris, J.R., Liang, J., Noble, P.W., and Hogan, B.L. (2011). Multiple stromal populations contribute to pulmonary fibrosis without evidence for epithelial to mesenchymal transition. Proc. Natl. Acad. Sci. USA *108*, E1475–E1483.

Savage, P., Blanchet-Cohen, A., Revil, T., Badescu, D., Saleh, S.M.I., Wang, Y.C., Zuo, D., Liu, L., Bertos, N.R., Munoz-Ramos, V., et al. (2017). A targetable EGFR-dependent tumor-initiating program in breast cancer. Cell Rep. *21*, 1140–1149.

Schultz, C.J., Torres, E., Londos, C., and Torday, J.S. (2002). Role of adipocyte differentiation-related protein in surfactant phospholipid synthesis by type II cells. Am. J. Physiol. Lung Cell. Mol. Physiol. *283*, L288–L296.

Sun, K.H., Chang, Y., Reed, N.I., and Sheppard, D. (2016). α-Smooth muscle actin is an inconsistent marker of fibroblasts responsible for force-dependent TGFβ activation or collagen production across multiple models of organ fibrosis. Am. J. Physiol. Lung Cell. Mol. Physiol. *310*, L824–L836.

Tahedl, D., Wirkes, A., Tschanz, S.A., Ochs, M., and Mühlfeld, C. (2014). How common is the lipid body-containing interstitial cell in the mammalian lung? Am. J. Physiol. Lung Cell. Mol. Physiol. *307*, L386–L394.

Thannickal, V.J., Zhou, Y., Gaggar, A., and Duncan, S.R. (2014). Fibrosis: ultimate and proximate causes. J. Clin. Invest. *124*, 4673–4677.

Thomas, A.Q., Lane, K., Phillips, J., 3rd, Prince, M., Markin, C., Speer, M., Schwartz, D.A., Gaddipati, R., Marney, A., Johnson, J., et al. (2002). Heterozygosity for a surfactant protein C gene mutation associated with usual interstitial pneumonitis and cellular nonspecific interstitial pneumonitis in one kindred. Am. J. Respir. Crit. Care Med. *165*, 1322–1328.

Thum, T. (2014). Noncoding RNAs and myocardial fibrosis. Nat. Rev. Cardiol. *11*, 655–663.

Torday, J.S., and Rehan, V.K. (2016). On the evolution of the pulmonary alveolar lipofibroblast. Exp. Cell Res. *340*, 215–219.

Tzouvelekis, A., and Kaminski, N. (2015). Epigenetics in idiopathic pulmonary fibrosis. Biochem. Cell Biol. *93*, 159–170.

Varisco, B.M., Ambalavanan, N., Whitsett, J.A., and Hagood, J.S. (2012). Thy-1 signals through PPARγ to promote lipofibroblast differentiation in the developing lung. Am. J. Respir. Cell Mol. Biol. *46*, 765–772.

von Gise, A., Stevens, S.M., Honor, L.B., Oh, J.H., Gao, C., Zhou, B., and Pu, W.T. (2016). Contribution of fetal, but not adult, pulmonary mesothelium to mesenchymal lineages in lung homeostasis and fibrosis. Am. J. Respir. Cell Mol. Biol. *54*, 222–230.

Wynn, T.A., and Ramalingam, T.R. (2012). Mechanisms of fibrosis: therapeutic translation for fibrotic disease. Nat. Med. *18*, 1028–1040.

Xiang, F.L., Fang, M., and Yutzey, K.E. (2017). Loss of β-catenin in resident cardiac fibroblasts attenuates fibrosis induced by pressure overload in mice. Nat. Commun. *8*, 712.

Xie, T., Liang, J., Liu, N., Huan, C., Zhang, Y., Liu, W., Kumar, M., Xiao, R., D'Armiento, J., Metzger, D., et al. (2016). Transcription factor TBX4 regulates myofibroblast accumulation and lung fibrosis. J. Clin. Invest. *126*, 3063–3079.

Yan, K.S., Gevaert, O., Zheng, G.X.Y., Anchang, B., Probert, C.S., Larkin, K.A., Davies, P.S., Cheng, Z.F., Kaddis, J.S., Han, A., et al. (2017). Intestinal enteroendocrine lineage cells possess homeostatic and injury-inducible stem cell activity. Cell Stem Cell *21*, 78–90.e6.

Yu, F., Jiang, Z., Chen, B., Dong, P., and Zheng, J. (2017). NEAT1 accelerates the progression of liver fibrosis via regulation of microRNA-122 and Kruppel-like factor 6. J. Mol. Med. (Berl.) *95*, 1191–1202.

Zepp, J.A., Zacharias, W.J., Frank, D.B., Cavanaugh, C.A., Zhou, S., Morley, M.P., and Morrisey, E.E. (2017). Distinct mesenchymal lineages and niches promote epithelial self-renewal and myofibrogenesis in the lung. Cell *170*, 1134–1148.e10.

**Cell Reports, Volume *22***

## Supplemental Information

# Single-Cell Deconvolution of Fibroblast Heterogeneity in Mouse Pulmonary Fibrosis

**Ting Xie, Yizhou Wang, Nan Deng, Guanling Huang, Forough Taghavifar, Yan Geng, Ningshan Liu, Vrishika Kulur, Changfu Yao, Peter Chen, Zhengqiu Liu, Barry Stripp, Jie Tang, Jiurong Liang, Paul W. Noble, and Dianhua Jiang**

**SUPPLEMENTAL INFORMATION**

# Single Cell Deconvolution of Fibroblast Heterogeneity in Mouse Pulmonary Fibrosis

Ting Xie, Yizhou Wang, Nan Deng, Guanling Huang, Forough Taghavifar, Yan Geng, Ningshan Liu, Vrishika Kulur, Changfu Yao, Peter Chen, Zhengqiu Liu, Barry Stripp, Jie Tang, Jiurong Liang, Paul W. Noble, Dianhua Jiang

## Supplemental Experimental Procedures

### Mouse lung fibrosis model

Adult mice (both male and female), 8 to 16 weeks old, were subjected to bleomycin-induced lung injury (Li et al., 2011; Liang et al., 2016; Xie et al., 2016). Bleomycin at 2.5 U/kg was injected intratracheally. Mouse lungs were harvested on day 21 for single-cell isolation.

### Flow cytometry

Fluorescence- activated cell sorting (FACS) experiments were performed using fresh lung preparations. Triple-heterozygous *αSMA-GFP;Tbx4-Cre;Rosa26-tdTomato* mouse lung homogenates for single-cell flow cytometry were prepared as previously described (Xie et al., 2016). Briefly, fresh mouse lungs were perfused with 10 ml PBS, elastase (4 U/ml; Worthington Biochemical Corporation) were injected through the trachea to inflate the

lung and dissociate epithelial cells. After that, samples were cut into approximately 1-3 mm pieces and digested with DNase I (100 U/ml; Sigma). Single cell homogenates were collected after passing through cell strainers and centrifugation. Flow cytometry was used to sort αSMA-GFP+tdTomato+, αSMA-GFP-tdTomato+, and αSMA-GFP-tdTomato- within live Epcam-CD31-CD45- MCs. Primary antibodies to CD31, and CD45, and secondary antibody anti-streptavidin were all from eBioscience (San Diego, CA). Mouse anti-EpCAM (G8.8, catalog 118215) were from BioLegend (San Diego, CA). 7-AAD was from BD Biosciences (San Diego, CA). Singlet discrimination was sequentially performed using plots for forward scatter (FSC-A versus FSC-H) and side scatter (SSC-W versus SSC-H). Dead cells were excluded by scatter characteristics and viability stains. All FACS experiments were performed on an Aria III sorter (BD Immunocytometry Systems, San Jose, CA) at the Cedars-Sinai Medical Center Shared FACS Facility and FACS data were analyzed using FlowJo software (TreeStar, Ashland, OR).

Single cell RNA-seq data analysis

Cell Ranger 1.3.1 (10X Genomics) was used to demultiplex reads and convert raw base call files into fastq format. Reads alignment was performed by using STAR (version 2.5.1) (Dobin et al., 2013) with default parameters, using a custom mouse mm10 transcriptome reference from Gencode Release M9 annotation, containing all protein coding and long non-coding RNA genes. Expression counts for each gene in all samples were collapsed and normalized to unique molecular identifier (UMI) counts using Cell Ranger 1.3.1 (10X Genomics). The result is a large digital expression matrix with cell barcodes as rows and gene identities as columns. We obtained 80,412 post-normalization mean reads per cell

with median genes per cell of 1,189 and median UMI counts per cell of 2,631. Cells of D0 were aggregated into a single database by using Cell Ranger 1.3.1 (10X GEnomics) as well as the cells from D21 samples. Depth normalization was performed before merging by subsampling reads from higher-depth libraries until they all have an equal number of confidently mapped reads per cell to reduce the batch effect introduced by sequencing. Mapping percentage of mitochondrial genes and total number of expressed for each cell was calculated by using Seurat suite version 2.0.0 (Butler, 2017; Macosko et al., 2015). Cells with percentage of reads mapped on mitochondrial genes > 15% or total number of genes expressed < 300 were removed from further analysis. 614 cells in d0 αSMA-GFP+tdTomato+ and 2835 cells in d21 αSMA-GFP+tdTomato+ sample, 1943 cells in d0 MCs and 3386 cells in d21 MCs sample were included for further analysis.

Expression of UMI counts for each gene were normalized by times the size factor calculated by median of total of UMI counts for all cells divided total of UMI counts for each cell. To obtain two-dimensional projections of the population's dynamics, principal component analysis (PCA) was firstly run on the normalized gene-barcode matrix to reduce the number of feature dimensions. Top 10 principle components (PC) that explained more variability than expected by chance were selected using a permutation-based test implemented in Seurat and passed to t-distribution stochastic neighbor embedding (tSNE) (Van Der Maaten, 2008) for clustering visualization by using Cell Ranger 1.3.1 (10X Genomics). For tSNE, the perplexity parameter and the parameter was set to 30 and 0.5, respectively while the other parameters were left as defaults and total iterations was 1000. A cloupe file was generated as input for a graphical user

interface browser, Loupe Cell Browser 1.0.5, to present the clustering of cell population and gene expression of identified marker genes.

In order to reduce any potential batch effect, we collected our samples at the same time and all the samples were processed for single cell RNA-seq on the same day. After construction of the single cell RNA-seq libraries, we performed aggregation analysis

Significantly differentiated gene analysis

sSeq (Yu et al., 2013) integrated in the Cell Ranger R kit version 2.0.0 was employed to identify the differentially expressed genes between groups of cells, which modeled gene expression with the Negative Binomial (NB) distribution using a shrinkage approach for dispersion estimation. Gene expression for each cluster was compared to other cells yielding a list of genes that are differentially expressed in that cluster relative to the rest of the sample. Benjamini-Hochberg procedure was used for multiple test corrections to calculate the adjusted p value. The adjusted p value, average expression in target cluster (main_a_sizenorm) and log2 fold change was considered side by side to pick up the significant genes. We set the cutoff of adjusted p-value <0.05, average expression > 1 and log2 fold change > 2, depending on the expression activity of samples and discrepancy among cells. And the method was keep consistent thought out all the MC subtypes.

DE genes which are exclusively expressed in each single MC subgroups were selected for top subgroup specific signature genes and used for drawing heat maps and violin plots by using ggplot2 v2.2.1 in R v3.3.1.

## Transcription factor analysis

Transcription factors were defined and annotated by RIKEN TFdb (The Institute of Physical and Chemical Research Transcription Factor Database), this list was further curated for missing genes and occasional mis-annotated transcription factors.

## lncRNA analysis

lncRNAs annotated by Ensembl biomart (Wellcome Trust Sanger Institute and European Bioinformatics Institute) were extracted from DE gene list for each MC subtypes.

## Extracellular and plasma membrane expressing gene analysis

Extracellular and plasma membrane expressing genes were identified according to COMPARTMENTS, a subcellular localization database (The Novo Nordisk Foundation Center for Protein Research (CPR), the Luxembourg Centre for Systems Biomedicine (LCSB), and the Commonwealth Scientific and Industrial Research Organization (CSIRO).).

## Customizable suite of single-cell R-analysis tools (SCRAT) analysis

SCRAT based on SOM machine learning (Camp et al., 2017) were used to determine and envision high-dimensional metagene sets exhibited in each population of MCs during fibrosis. Sample trajectory analysis was also performed by SCRAT suite inputting 5 MC subtypes with cell cycle correction.

We applied the Scater R package (McCarthy et al., 2017) to conduct quality control on the cells and low-abundance gene filtering (Lun et al., 2016b). We removed low-quality cells based on three criteria: 1) cells with log-library sizes more than 2 median absolute deviations (MADs) below the median; 2) cells with log-transformed number of expressed genes 2 MADs below median; 3) cells with mitochondrial proportions 2 MADs higher than median. Low-abundance genes with an average UMI count below 0.2 were filtered out. The data was then cell-specifically normalized with pool-based size factors (Lun et al., 2016a).

**Key Resource Table**

| REAGENT or RESOURCE | SOURCE | IDENTIFIER |
|---|---|---|
| Antibodies | | |
| Anti-Epcam | eBioscience | 118216 |
| Anti-CD31 | eBioscience | 102404 |
| Anti-CD45 | eBioscience | 103104 |
| Anti-biotin-APC-eFlour780 | eBioscience | 47-4317-82 |
| Chemicals, Peptides, and Recombinant Proteins | | |
| Bleomycin | Hospira | NDC61703-332-18 |
| Elastase | Worthington Biochemical Corporation | LS002280 |
| DNase I | Sigma | D4527 |
| 7-AAD | BD Biosciences | 51-68981E |
| Chromium Single Cell 3′ v2 Reagent Kits | 10x Genomics | 120234 |
| SPRIselect Reagent Kit | Beckman Coulter | B23318 |
| Chromium Single-Cell 3′ Library Kit | 10x Genomics | 120237 |
| KAPA Library Quantification Kit | KAPA Biosystems | KK4824 |
| Deposited Data | | |
| Raw data files of the RNA sequencing analyses | GEO | GSE104154 |
| Experimental Models: Organisms/Strains | | |
| αSMA-GFP *Tbx4-Cre Rosa26-tdTomato* mouse strain with C57BL/6 background | Cedars-Sinai Comparative Medicine | |

| Software and Algorithms | | |
|---|---|---|
| Cell Ranger 1.3.1 | 10X Genomics | version 1.3.1 |
| STAR | Dobin et al., 2013 | version 2.5.1 |
| Seurat suite | Butler, 2017, Macosko et al., 2015 | version 2.0.0 |
| Loupe Cell Browser | 10X Genomics | version 1.0.5 |
| Cell Ranger R kit | 10X Genomics | version 2.0.0 |
| ggplot2 | R Core Team | version 2.2.1 in R v3.3.1 |
| RIKEN TFdb | The Institute of Physical and Chemical Research Transcription Factor Database | |
| Ensembl biomart | Wellcome Trust Sanger Institute and European Bioinformatics Institute | |
| COMPARTMENTS | The Novo Nordisk Foundation Center for Protein Research (CPR), the Luxembourg Centre for Systems Biomedicine (LCSB), and the Commonwealth Scientific and Industrial Research Organization (CSIRO) | |
| SCRAT | Camp et al., 2017 | |
| Scater R package | McCarthy et al., 2017 | |

**Reference:**

Butler, A., Satija, R. (2017). Integrated analysis of single cell transcriptomic data across conditions, technologies, and species. BioRxiv.

Camp, J.G., Sekine, K., Gerber, T., Loeffler-Wirth, H., Binder, H., Gac, M., Kanton, S., Kageyama, J., Damm, G., Seehofer, D.*, et al.* (2017). Multilineage communication regulates human liver bud development from pluripotency. Nature *546*, 533-538.

Dobin, A., Davis, C.A., Schlesinger, F., Drenkow, J., Zaleski, C., Jha, S., Batut, P., Chaisson, M., and Gingeras, T.R. (2013). STAR: ultrafast universal RNA-seq aligner. Bioinformatics *29*, 15-21.

Li, Y., Jiang, D., Liang, J., Meltzer, E.B., Gray, A., Miura, R., Wogensen, L., Yamaguchi, Y., and Noble, P.W. (2011). Severe lung fibrosis requires an invasive fibroblast phenotype regulated by hyaluronan and CD44. J Exp Med *208*, 1459-1471.

Liang, J., Zhang, Y., Xie, T., Liu, N., Chen, H., Geng, Y., Kurkciyan, A., Mena, J.M., Stripp, B.R., Jiang, D.*, et al.* (2016). Hyaluronan and TLR4 promote surfactant-protein-C-positive alveolar progenitor cell renewal and prevent severe pulmonary fibrosis in mice. Nat Med *22*, 1285-1293.

Lun, A.T., Bach, K., and Marioni, J.C. (2016a). Pooling across cells to normalize single-cell RNA sequencing data with many zero counts. Genome Biol *17*, 75.

Lun, A.T., McCarthy, D.J., and Marioni, J.C. (2016b). A step-by-step workflow for low-level analysis of single-cell RNA-seq data with Bioconductor. F1000Res *5*, 2122.

Macosko, E.Z., Basu, A., Satija, R., Nemesh, J., Shekhar, K., Goldman, M., Tirosh, I., Bialas, A.R., Kamitaki, N., Martersteck, E.M.*, et al.* (2015). Highly Parallel Genome-wide Expression Profiling of Individual Cells Using Nanoliter Droplets. Cell *161*, 1202-1214.

McCarthy, D.J., Campbell, K.R., Lun, A.T., and Wills, Q.F. (2017). Scater: pre-processing, quality control, normalization and visualization of single-cell RNA-seq data in R. Bioinformatics *33*, 1179-1186.

Van Der Maaten, L.H., G. (2008). Visualizing data using t-SNE. Journal of Machine Learning Research *9*, 2579--2605.

Xie, T., Liang, J., Liu, N., Huan, C., Zhang, Y., Liu, W., Kumar, M., Xiao, R., D'Armiento, J., Metzger, D.*, et al.* (2016). Transcription factor TBX4 regulates myofibroblast accumulation and lung fibrosis. J Clin Invest *126*, 3063-3079.

Yu, D., Huber, W., and Vitek, O. (2013). Shrinkage estimation of dispersion in Negative Binomial models for RNA-seq experiments with small sample size. Bioinformatics *29*, 1275-1282.

# Supplementary Fig. 1

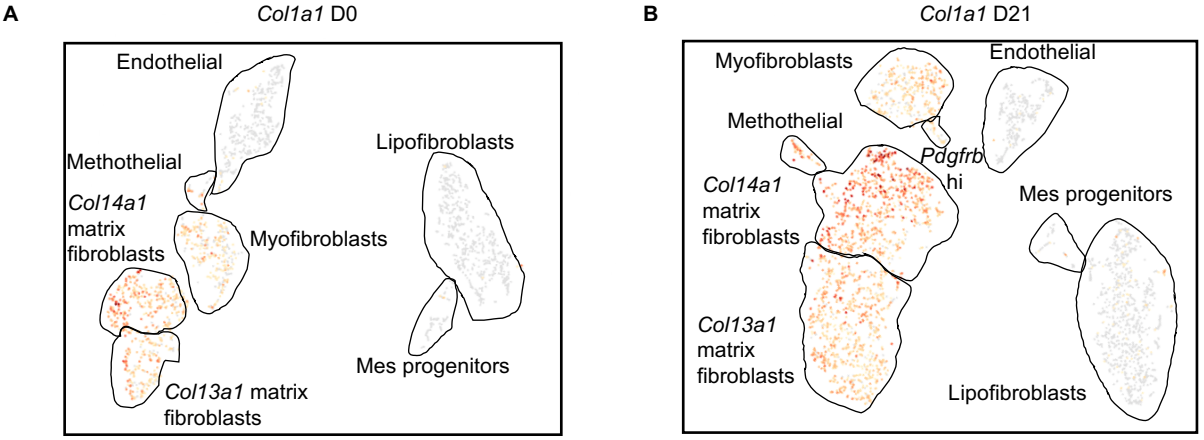


Supplementary fig. 1 *Col1a1* expression visualized in t-SNE plot. Related to Figure 3. (A-B) *Col1a1* expressing cells are scattered in Col13a1 and Col14a1 matrix fibroblasts, myofibroblasts, methothelial, and pdgfrb hi cells, and *Col1a1* highly expressing cells are matrix fibroblasts in both normal (A) and fibrotic (B) MCs.

# Supplementary Fig. 2

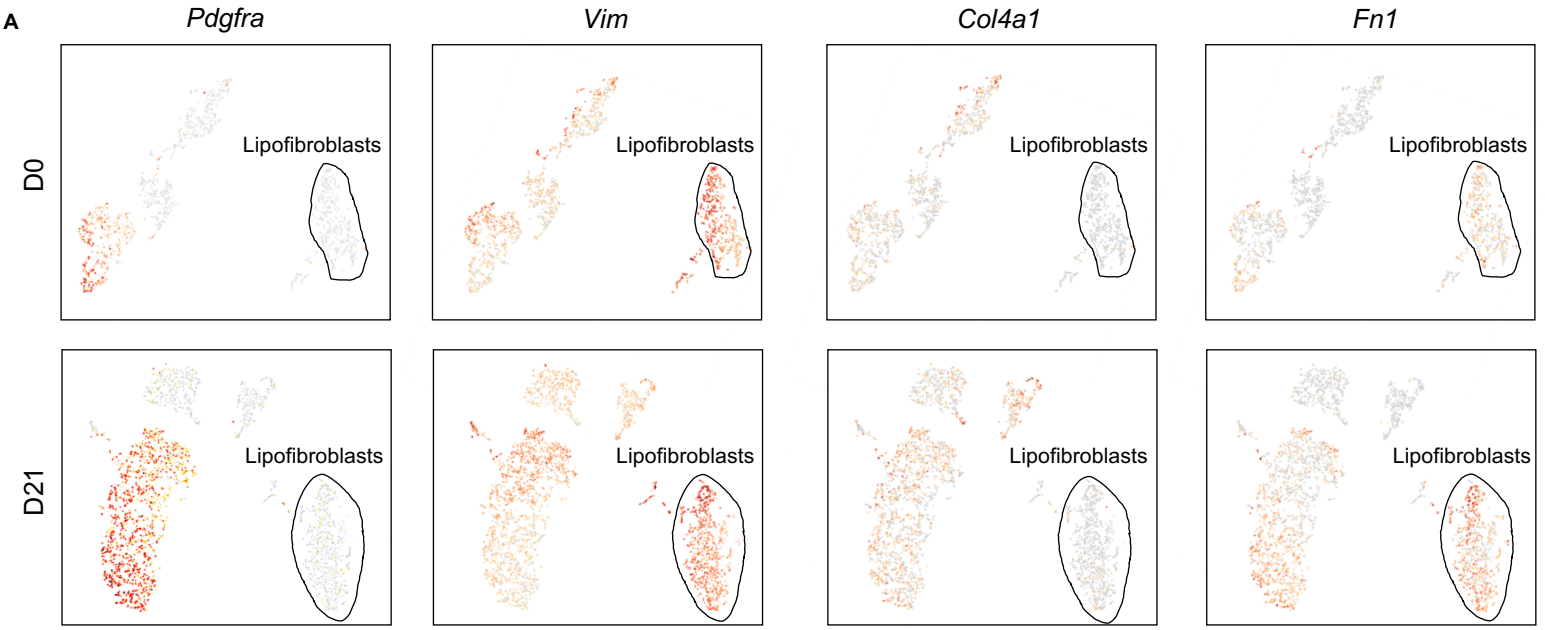


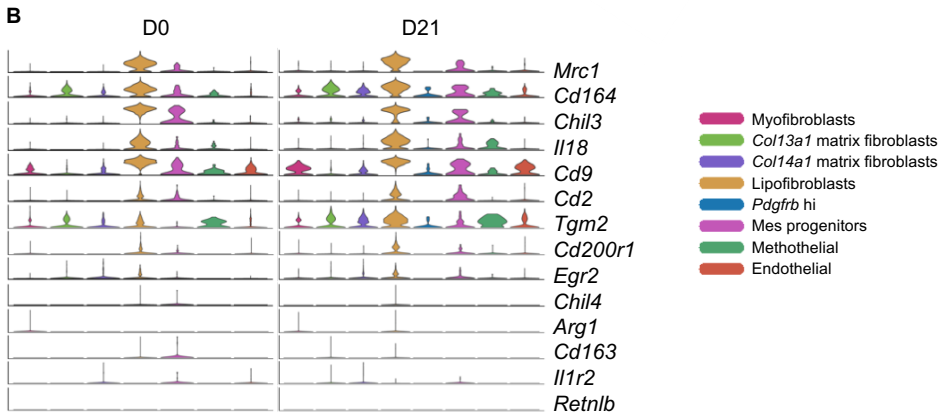


Supplementary fig. 2 Lipofibroblasts features M2-like macrophage genes. Related to Figure 5. (A) *Pdgfra, Vim, Col4a1, and Fn1* expression in MC subtypes. (B) M2-like genes were examined across all MC subtypes.

# Supplementary Fig. 3

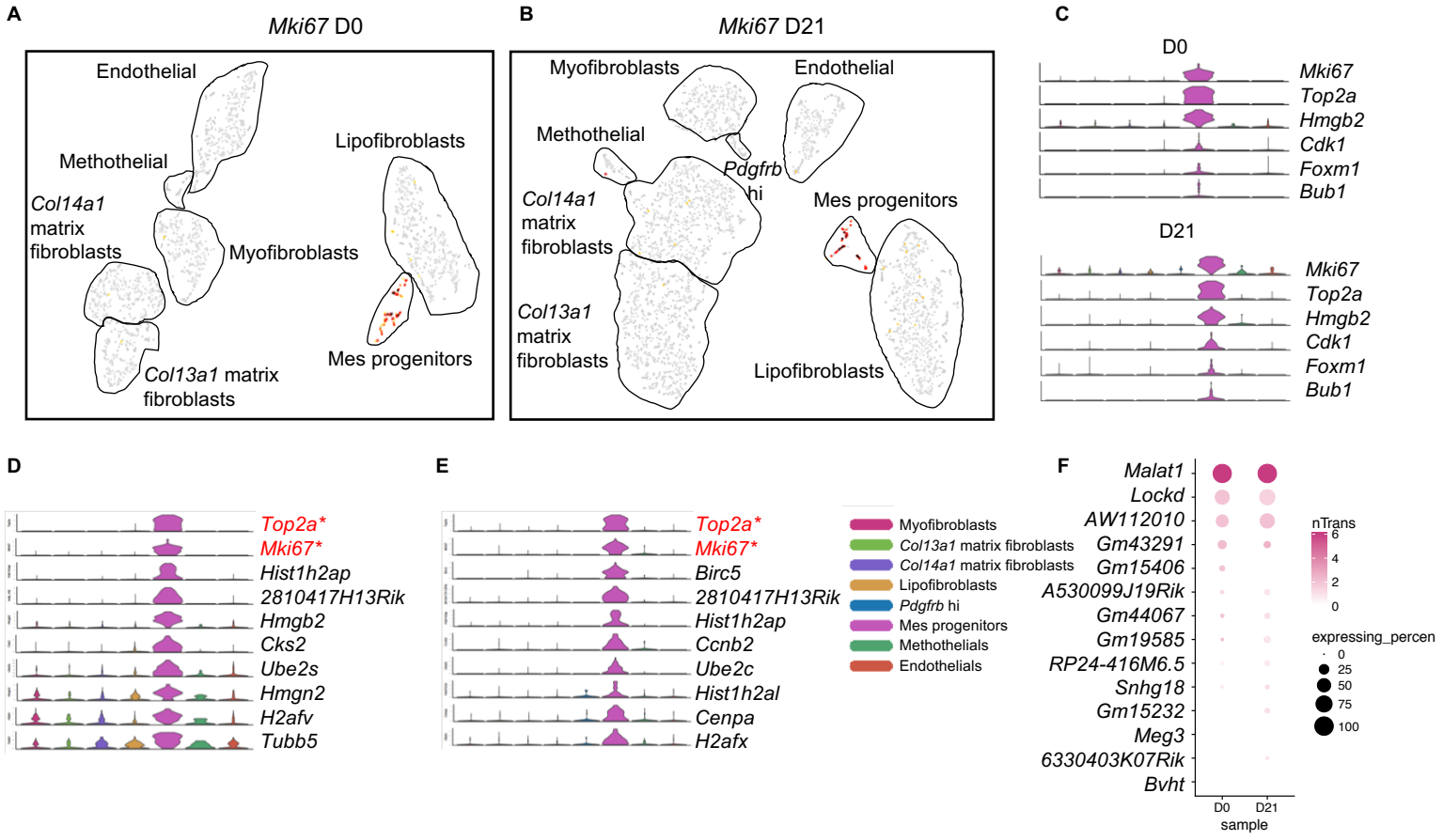


Supplementary fig. 3 Gene profile distinguishes mesenchymal progenitors. Related to Figure 1. (A-B) *Mki67* expression shown in t-SNE plot of all MC subtypes in both normal and fibrotic conditions. (C) Known mesenchymal progenitor marker expression across MC subtypes. (D-E) Enrichment pattern of genes in mesenchymal progenitors cross all MC subtypes. (F) Mesenchymal progenitor lncRNA expression. (G) Heat map showing top differential expression of genes labeled with cellular locations in normal and fibrotic condition. (H) *Hmgb2* as the most significantly expressed transcription factor in mesenchymal progenitor subtype by violin plot. (I) Top transcription factors were compared between normal and fibrotic status in this subtype.

# Supplementary Fig. 4

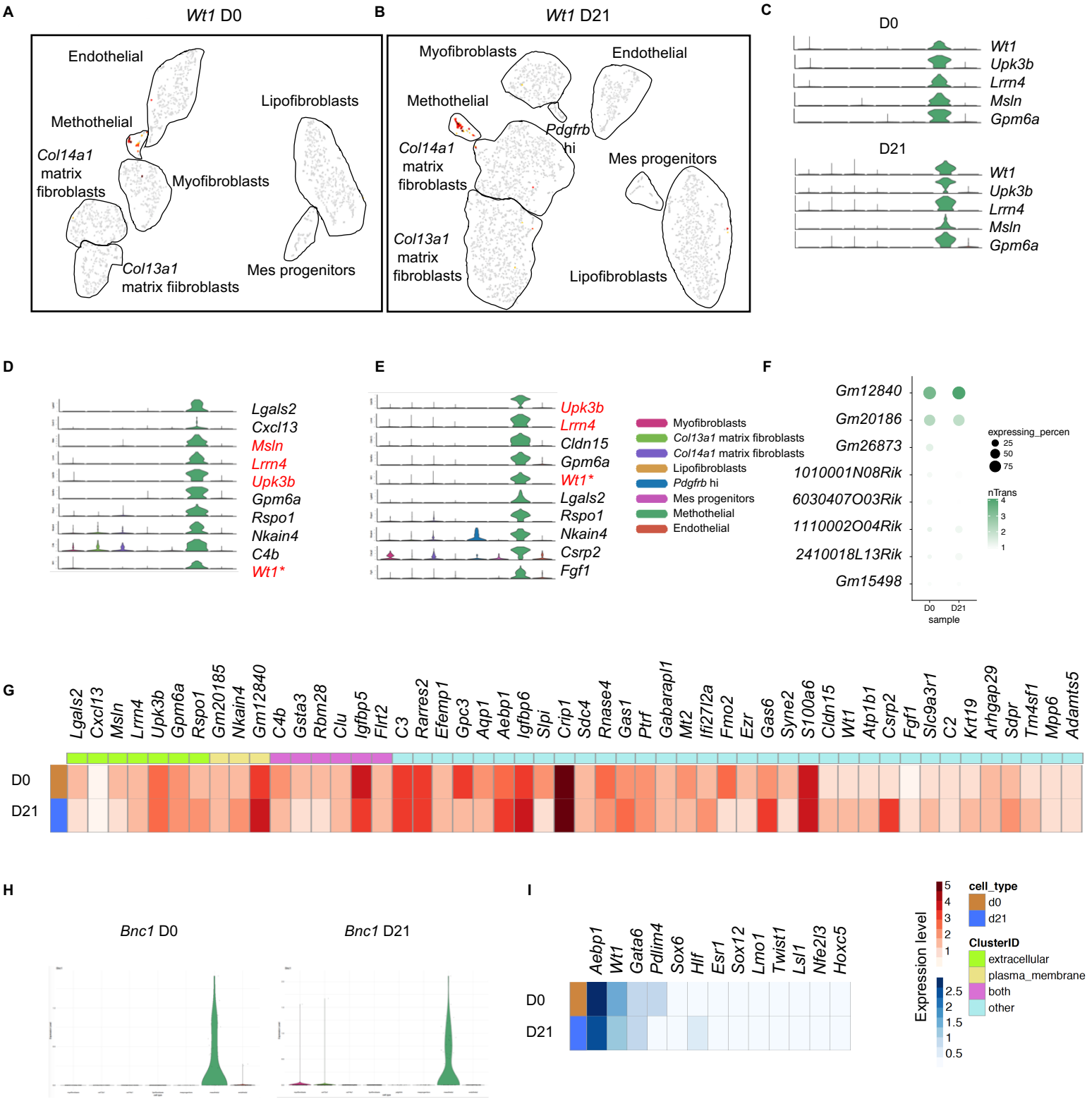


Supplementary fig. 4 Analysis of gene sets in mesothelial cells. Related to Figure 1. (A-B) *Wt1* marks exclusively the mesothelial cell cluster. (C) Known mesothelial markers were enriched in this cluster. (D-E) Top signature genes were exhibit across MC subtypes as violin plots. (F) Top IncRNAs were analyzed. (G) Comparison of normal and fibrotic top 50 significant genes were demonstrated as heat map. (H) *Bnc1* as the most discriminative transcription factors. (I) Comparison of top expressed transcription factors in mesothelial cell subtype.

# Supplementary Fig. 5

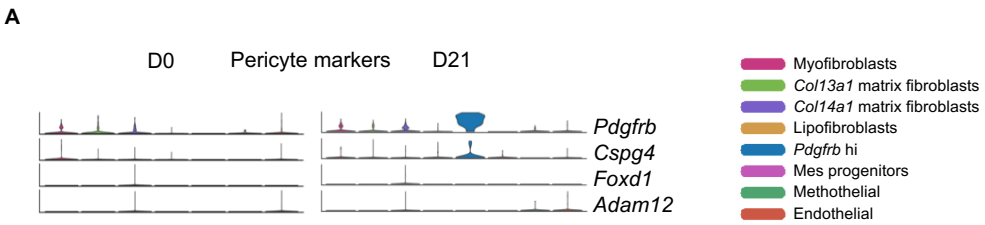


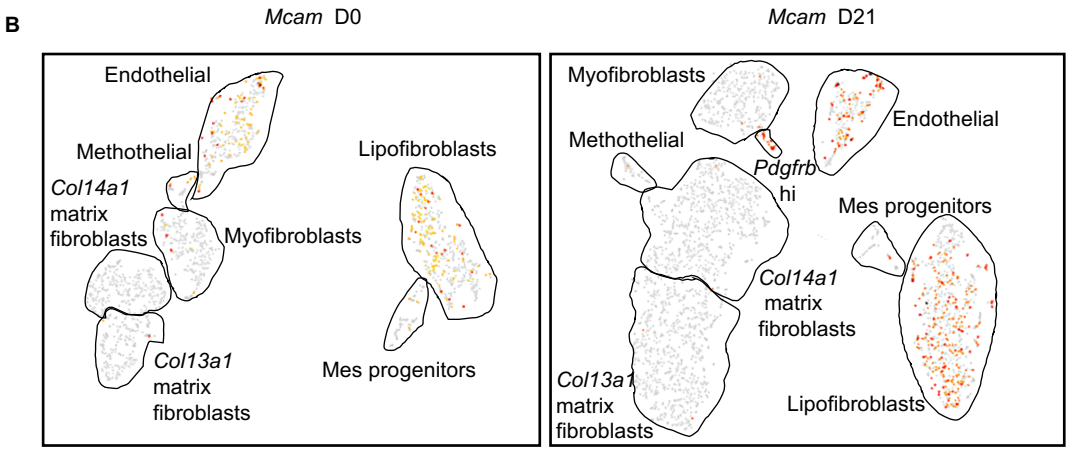


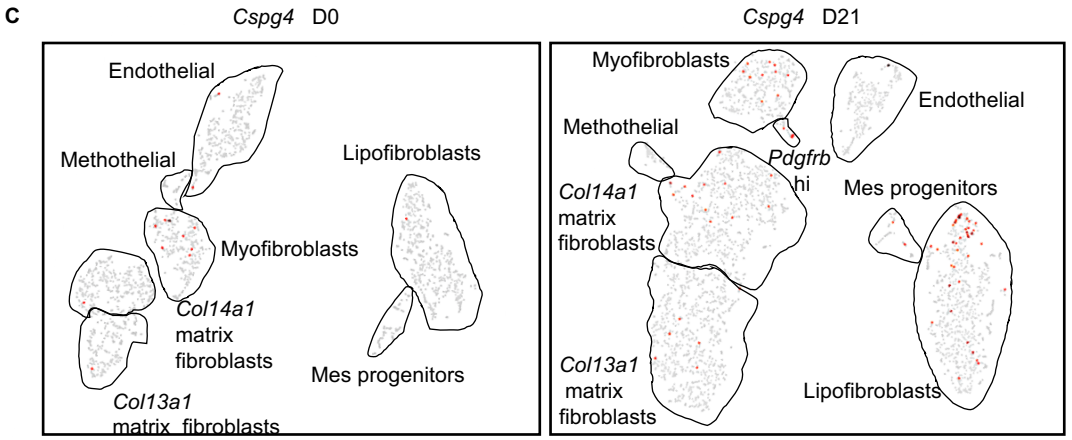


Supplementary fig. 5 Known pericyte markers examination. Related to Figure 6. (A) Violin plots shown previously reported pericyte markers (*Pdgfrb, Cspg4, Foxd1,* and *Adam12*) across all MC subtypes. (B-C) t-SNE projection and single cell expression pattern of *Mcam* (B) and *Cspg4* (C).

# Supplementary Fig. 6

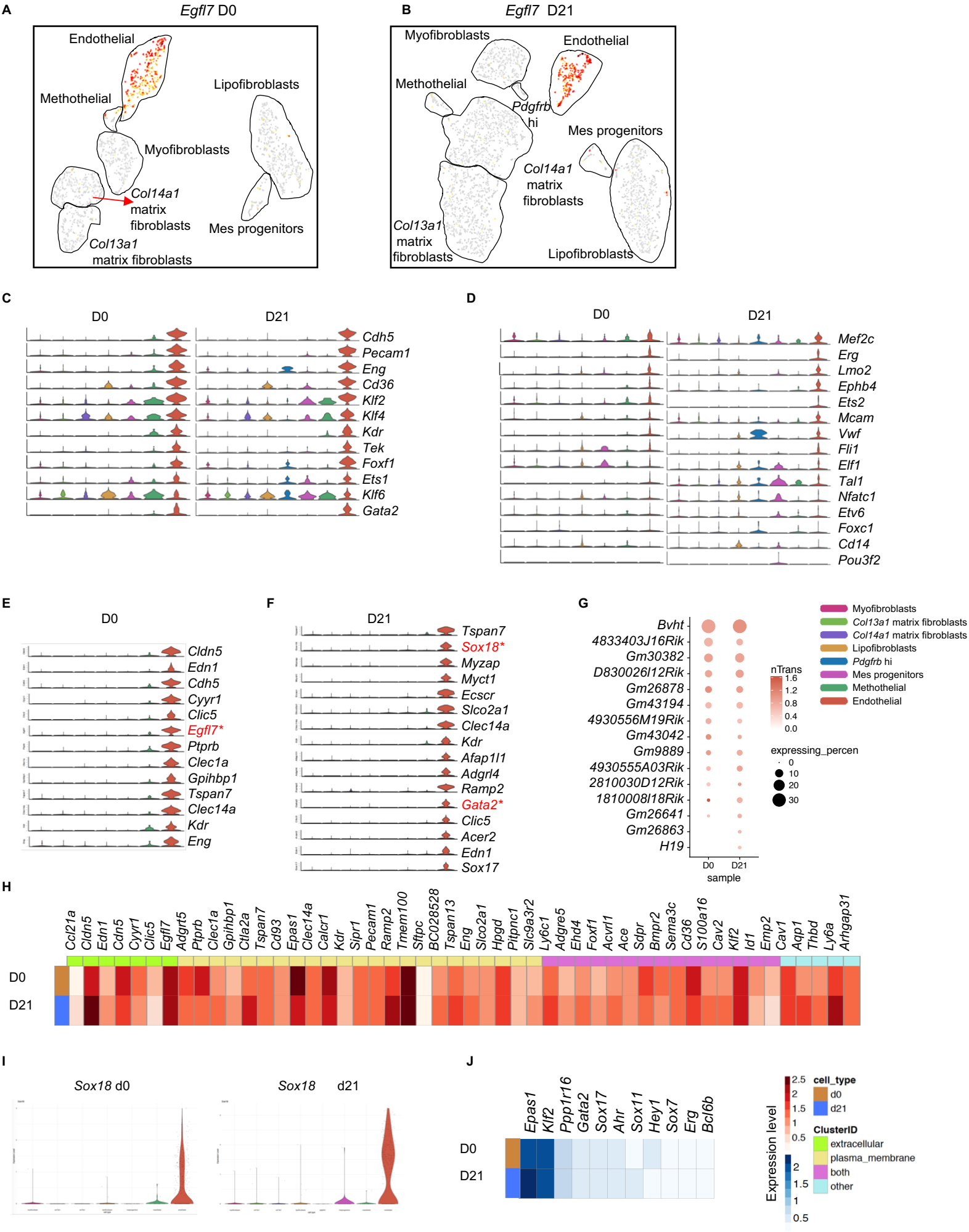

Supplementary fig. 6 Exploration of endothelial cell markers, lncRNAs, and transcription factors. Related to Figure 1. (A-B) Distinct cluster of *Egfl7* highly expression cells in MC subtypes. (C-D) Previously reported endothelial cell markers are significantly expressed in this cluster. (E-F) Violin plots showing expression of known and novel endothelial signature genes. (G) Top lncRNAs in endothelial subtype. (H) Top 50 differentially expressed genes in endothelial subtype were compared between corresponding conditions. (I) The most discriminative transcription factor *Sox18* expression by violin plot. (J) Heat map visualization of top unique transcription factors between normal and fibrotic endothelial cells in MCs.

# Supplementary Fig. 7

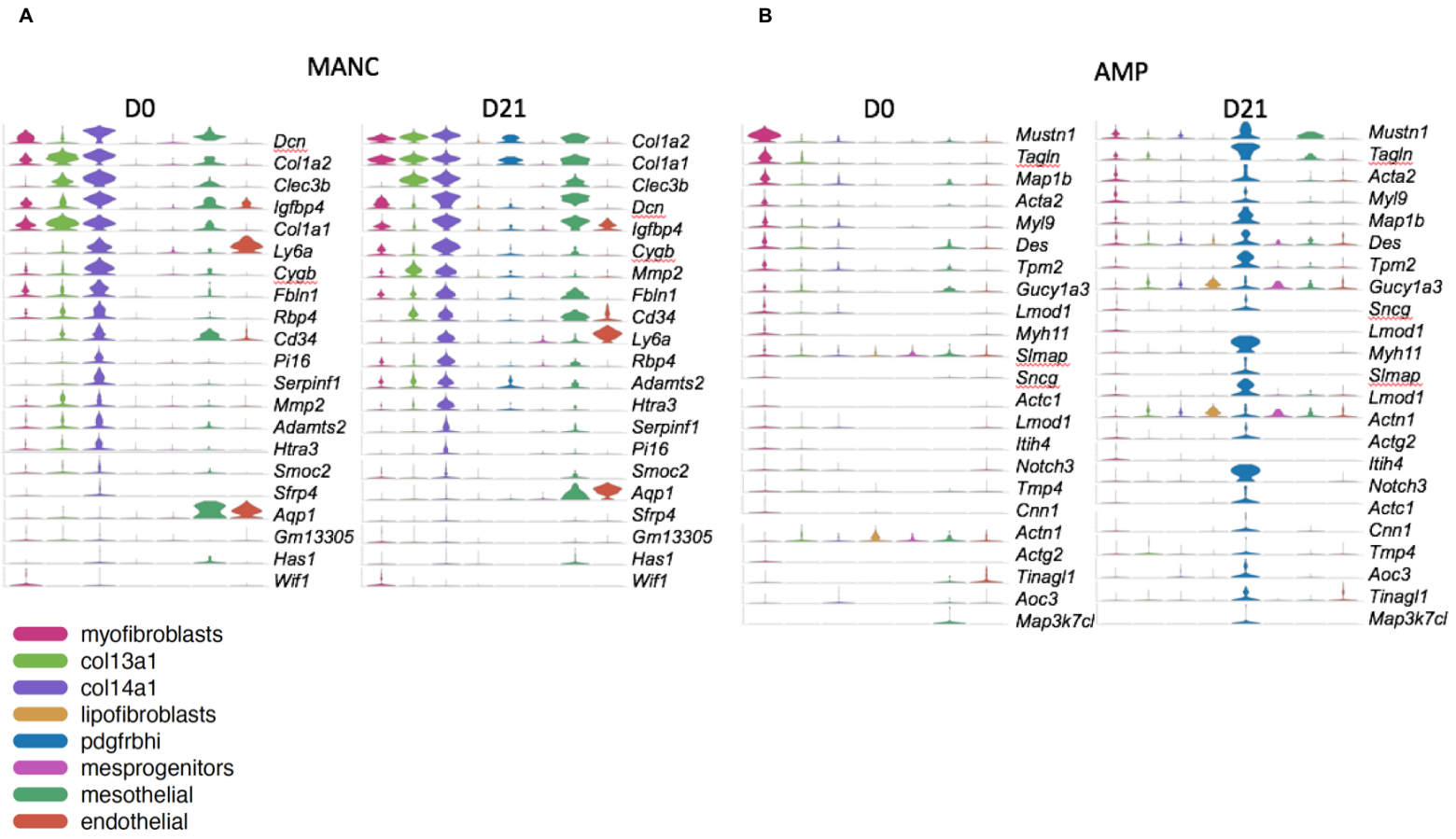


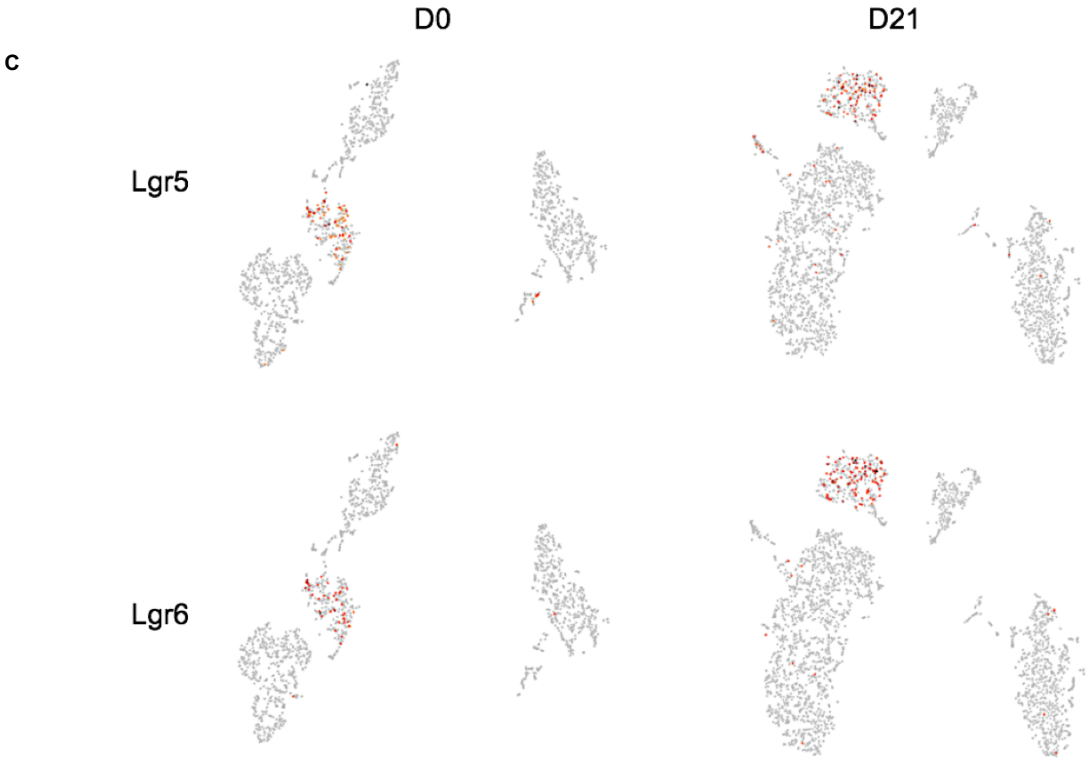


Supplementary fig. 7 MANCs, AMP, Lgr5 and Lgr6 mesenchymal subpopulation signature gene comparisons. Related to Figure 1. (A) Violin plots shown previously reported MANC markers across all MC subtypes. (B) Violin plots shown previously reported AMP markers across all MC subtypes. (C) t-SNE projection and single cell expression pattern of *Lgr5* and *Lgr6*.